

Detached Red Giant Eclipsing Binary Twins: Rosetta Stones to the Galactic Bulge

D.M. Nataf, A. Gould and M.H. Pinsonneault

Department of Astronomy, Ohio State University, 140 W. 18th Ave., Columbus,
OH 43210, USA

e-mail: (nataf,gould,pinsono)@astronomy.ohio-state.edu

Received March 24, 2012

ABSTRACT

We identify 34 highly-probable detached, red giant eclipsing binary pairs among 315 candidates in Devor’s catalog of ≈ 10000 OGLE-II eclipsing binaries. We estimate that there should be at least 200 such systems in OGLE-III. We show that spectroscopic measurements of the metallicities and radial-velocity-derived masses of these systems would independently constrain both the age-metallicity and helium-metallicity relations of the Galactic bulge, potentially breaking the age-helium degeneracy that currently limits our ability to characterize the bulge stellar population. Mass and metallicity measurements alone would be sufficient to immediately validate or falsify recent claims about the age and helium abundance of the bulge. A spectroscopic survey of these systems would constrain models of Milky Way assembly, as well as provide significant auxiliary science on research questions such as mass loss on the red giant branch. We discuss the theoretical uncertainties in stellar evolution models that would need to be accounted for to maximize the scientific yield.

Key words: *Galaxy: bulge – Galaxy: stellar content – binaries: eclipsing*

1. Introduction

To understand the origin and evolution of the Galactic bulge, one would like to measure the age, kinematics, and abundances for a large and representative sample of stars. Because both photometric and spectroscopic ages are strongly degenerate with helium abundance (Marín-Franch *et al.* 2010, Nataf and Gould 2011), it is absolutely essential that each star in such a sample have an estimate of its helium content, in addition to the “metal” abundances that are more usually reported. This appears to be a daunting requirement: despite the fact that helium comprises 25–40% of the baryonic mass of bulge stars, there are no reported spectroscopic helium estimates, other than that of the stripped B-star S2 orbiting the supermassive black hole at the center of our Galaxy (Martins *et al.* 2008). Helium is simply too tightly bound to give rise to detectable lines in the relatively cool stars that inhabit the

bulge, though the application of Herculean techniques to the HeI 10830 has shown promise in the case of the metal-poor globular cluster NGC 2808 (Pasquini *et al.* 2011).

Here we argue that well-detached double-red-giant eclipsing binaries can provide a large $O(10^2)$ sample of such well-characterized stars. The choice of double-red-giant eclipsing binaries is far from obvious. Red giants (RGs) of luminosity comparable to the red clump (RC) are themselves relatively rare, roughly one per $10^3 M_{\odot}$. And it is straightforward to show that only $O(10^{-5})$ of these have detached eclipsing secondaries of comparable size. So, for example, one does not expect even one such binary in the entire system of Milky Way globular clusters. Detached eclipsing turnoff stars are at least 1000 times more plentiful. However, these systems do exist and are accessible once one has access to photometric surveys as large as OGLE: We note the recent detailed investigation of $3.5 M_{\odot}$ RG twins in a 371.6 day orbit, OGLE SMC113.3 4007 (Graczyk *et al.* 2012).

Nevertheless, for the specific problem of tracing the bulge population, double-RG eclipsing binaries are very much preferred. The principal reason is simply that they are brighter and hence all measurements are much more precise given instrumentation available currently or in the foreseeable future. For example, currently it is possible to obtain detailed spectroscopic abundances for turnoff stars only when they are highly magnified (Bensby *et al.* 2010, 2011). For the same reason, precision radial velocity (RV) measurements, needed for accurate masses, are extremely costly for turnoff stars. Even photometric light curves, which are required to measure the mean density of the system, are challenging (*e.g.*, Clarkson *et al.* 2011). This is not just because of the low flux levels of the source but more fundamentally, irreducible blending by ambient stars, as well as third bodies that are frequently present in close-binary systems (Tokovinin *et al.* 2006, Pribulla and Rucinski 2006). Finally, because the bulge has finite depth ($\sigma_{(m-M)_0} \approx 0.15$ mag) and is subject to differential extinction, one cannot, in strong contrast to globular clusters, use photometric information to precisely determine the phase of stellar evolution of a given turnoff star.

All of these problems are greatly reduced in RGs. Plentiful photons easily yield high signal-to-noise ratio (S/N) measurements. Blending is intrinsically less important because the sources are bright, and moreover it is possible to detect blends down to very low flux levels. High flux levels and low-blending imply that proper motions are more precisely measured, and precise light curves enable accurate distance measurements using standard eclipsing-binary techniques (at least to determine relative positions within the bulge). Finally, the whole phase of RG evolution is short, so that the phase of stellar evolution can be determined extremely precisely. The only real problem is the low frequency of detached double-red-giant eclipsing binaries. However, in this paper we show that at least 34 such systems are already present in the eclipsing-binary catalog constructed by Devor (2005) from OGLE-II data.

The structure of this paper is as follows. In Section 2, we show how to identify Galactic bulge RG EB twins from an order of magnitude larger list of candidates. The observed frequency of these systems in OGLE-II implies that there are of order 200 more waiting to be discovered in OGLE-III data. In Section 3, we summarize the stellar models used in this work. In Section 4, we discuss the immediate science that could be achieved with even preliminary spectroscopic follow-up. We find that mass and metallicity measurements would, by themselves, be sufficient to validate or falsify several hypotheses of the bulge stellar population. In Section 5, we investigate how well the system parameters must be measured and how the precision of these measurements translate into errors on the age-helium plane. Further, we show that if current theoretical and observational uncertainties on the RG temperature scale are reduced in the future, and if tidal effects could be taken into account by either selecting very detached systems or effectively modeling them, detached RG eclipsing binaries could in and of themselves be sufficient to fully characterize the Galactic bulge age-helium-metallicity relationship.

2. At Least 34 Detached Red Giant Eclipsing Binary Pairs in the OGLE-II Eclipsing Binary Catalog

There are significant challenges in finding RG eclipsing binary pairs. First, the lifetime of the RG phase is only $\approx 1\%$ of the stellar lifetime, which means that the two masses can differ by no more than $\approx 0.5\%$ for both stars to be in the RG phase simultaneously. Second, from Newton's generalization of Kepler's third law:

$$\left(\frac{a}{10 R_{\odot}}\right) = 0.84 \left(\frac{P}{2 \text{ days}}\right)^{2/3} \left(\frac{M_1 + M_2}{2 M_{\odot}}\right)^{1/3}, \quad (1)$$

it follows that RG eclipsing binary pairs will not be detached for the short orbital periods that are the most easily detected, due to their large physical size. Meanwhile, at longer periods, the geometrical probability of eclipse will go down as the inverse of the orbital separation, and even for fortuitous alignments for which $\sin i \approx 1$, the S/N will drop sharply with increased orbital separation as there will be fewer completed periods to phase the light curve over.

It is therefore not surprising that a photometric database as large as that of OGLE is required to produce a catalog of these systems. Devor (2005) combed through 218 699 variable stars in the OGLE-II bulge photometric survey, to identify 10 862 eclipsing binaries. There were 3 170 classified as detached eclipsing binaries, the overwhelming majority of which are foreground main-sequence disk stars. The top-left panel of Fig. 1 shows the dereddened color and magnitude of the 3 170 detached eclipsing binaries overplotted on a dereddened OGLE-III CMD of Baade's window (Szymadłowski *et al.* 2011). Only 315 of the catalog members have dereddened color $(V - I)_0 \geq 0.7$ mag and $P \geq 2$ days.

Though each of these candidates appear as RGs on the CMD and have eclipsing binary light curves, many are not true RG eclipsing binaries. We find that

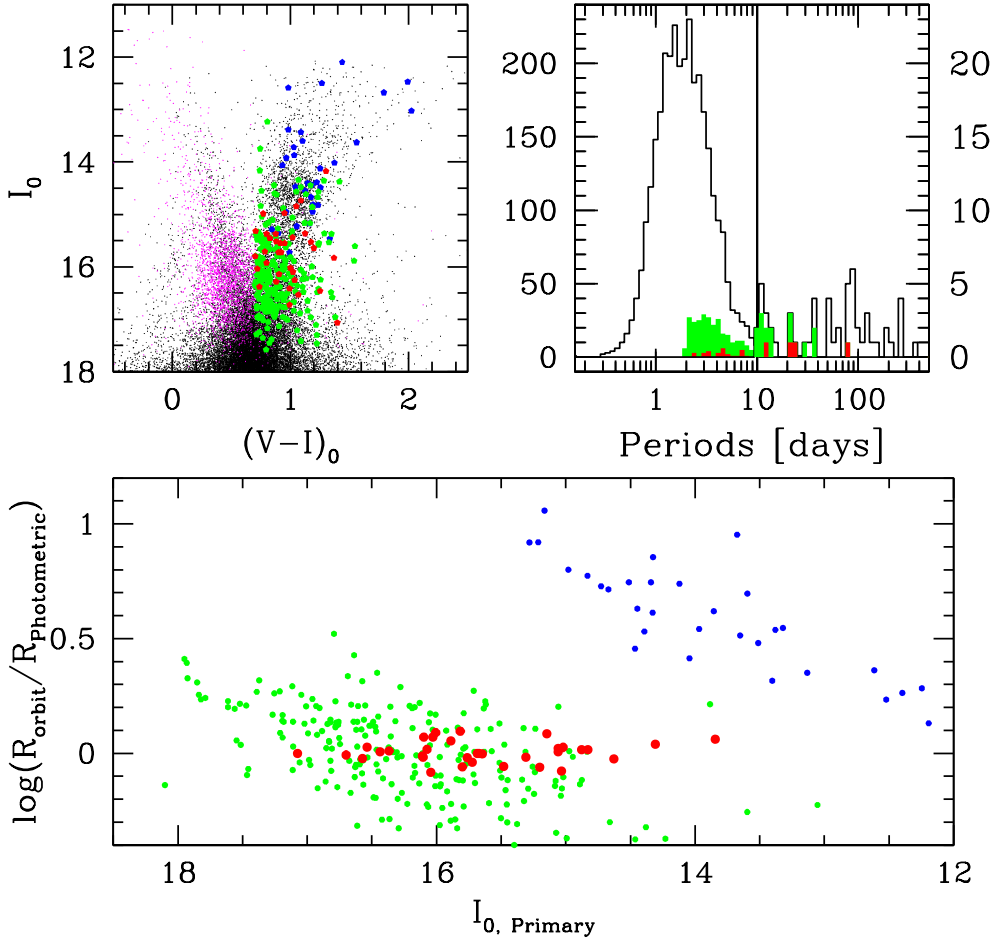


Fig. 1. At least 34 of the 10 862 OGLE-II eclipsing binary candidates in the catalog of Devor (2005) are detached RG eclipsing binary pairs. *Top-left*: dereddened color and magnitude of detached binaries (magenta), “gold”, “silver”, and spurious eclipsing binary sources with $(V-I)_0 \geq 0.7$ mag and $P \geq 2$ days (red, green, blue respectively), overplotted on a dereddened OGLE-III CMD toward Baade’s window (black). *Top-right*: histogram of period distribution of 3 170 detached eclipsing binaries, with the distribution of periods greater than 10 days enlarged. *Bottom*: comparison of stellar radii derived from the photometric and orbital information for the primary stars as a function of $I_{0, \text{Primary}}$. Same color scheme as *top-left*. The gold candidates pass the test of having consistent radii from photometry and orbital parameters.

at least 33 of these 315 candidates have unphysical parameters, as determined by deriving radius estimates. The solutions of Devor (2005) include the orbital periods and the ratios $R_{1,2}/a$, allowing estimates of the primary’s physical radius, $r = 5.30R_{\odot}(r_1/a)(P/\text{days})^{2/3}$, where we have assumed $M_1 + M_2 = 2 M_{\odot}$. This assumption of the mass will not contribute significant error due to the small value of the exponent: $1/3$. An independent estimate of the radii of these stars can be derived photometrically, by de-reddening their colors and magnitudes assuming an intrinsic color and brightness of the red clump (RC) $(V-I, I)_{\text{RC}} = (1.06, -0.10)$,

$(m - M)_{0,\text{bulge}} = 14.52$ and using the empirical color-surface-brightness relations of Kervella *et al.* (2004), by first transforming $(V - I)$ to $(V - K)$ using the *VIK* color-color relation of Bessell and Brett (1988). The results of this comparison are shown in the bottom panel of Fig. 1. There is a sequence of sources, plotted in blue, for which the ratio $R_{\text{orbit}}/R_{\text{photometric}}$ reaches values as high as 10. These are manifestly unphysical, and they comprise $\approx 10\%$ of the eclipsing-binary candidates with $(V - I)_0 \geq 0.7$ mag and $P \geq 2$ days. That these form a sequence strongly implies that they are a specific class of variables that happen to strongly resemble eclipsing binaries. We note that they are all as bright or brighter than the RC.

The 34 red points, which we call the “gold sample”, have a minimal size criterion $R_{\text{secondary}} \geq 3R_{\odot}$ (to ensure that both members are RG stars), and a consistent size criterion $|\log(R_{\text{primary,orbit}}/R_{\text{primary,photometric}})| \leq 0.10$, equivalent to a $\approx 25\%$ error in the radius or 0.5 mag in the brightness. This is an estimate of the effects due to errors in the corrections between color and surface brightness, differential reddening, and depth relative to the Galactocentric distance. 248 of the candidates, plotted in green, have properties that are physical but not optimal. Many are likely disk stars, other may have secondaries on the subgiant branch, for which follow-up analysis would not be able to assume $M_1 = M_2$. We classify these as the “silver” sample. We directly inspected each of the 34 gold eclipsing binary light curves by downloading photometry from the OGLE-II archive (Udalski *et al.* 1997, Szymadłowski *et al.* 2005). The OGLE-II light curves for the gold-sample candidates are shown in Figs. 2, 3, and 5. Both “gold” and “silver” candidates are listed in Tables 1 and 2 (in Appendix).

There may be more such systems to be found at brighter magnitudes. It has been demonstrated that there is a substantial population of undiscovered, bright periodic variables toward the Galactic bulge. However, OGLE photometry, from which the eclipsing binary candidates are derived, saturates at $I \approx 13$ mag (Szymadłowski *et al.* 2005). Nataf *et al.* (2009), as part of a microlensing feasibility study investigating bright ($8 \lesssim I \lesssim 13$) stars toward the Galactic bulge, took 151 exposures spanning 88 nights and estimated that 50% of the periodic variables were not previously detected. Due to the short baseline, it is not surprising that no long-period detached eclipsing binaries are present in the catalog of 52 previously undetected eclipsing binaries (Nataf *et al.* 2010), but it is likely that a few could be found near the tip of the RG branch by a dedicated campaign with a small-aperture telescope.

2.1. Uncertainties in the Photometric Parameters

We comment on a few uncertainties in the parameters derived by Devor (2005) and how they can be rectified.

The first is that of ellipsoidal variations, which are not accounted for. Ellipsoidal variations result from the geometric distortion of close eclipsing binary stars due to their mutual gravitation. That this was not taken into account by Devor

(2005) likely results in small errors in some of the parameters such as the stellar densities. However, this effect could be well approximated for in a more detailed study.

To better understand these effects, we follow the derivation of Assef *et al.* (2006). From Eq. (6) of Morris (1985), the mean magnitude difference between maxima and minima resulting from ellipsoidal variations, ΔM , behaves as:

$$\Delta M = 0.325 \frac{(\tau_1 + 1)(15 + \mu_1)}{(3 - \mu_1)} \left(\frac{m_2}{m_1} \right) \left(\frac{R_1}{a} \right)^3 \sin^2 i \quad (2)$$

where μ_1 is the primary's linear limb-darkening coefficient and τ_1 is the primary's gravity-darkening coefficient. From Table 1 of Al-Naimiy (1978), we find $\mu_1 \approx 0.6$, and $\tau_1 \approx 0.4$ from Al-Naimiy (1978) and Eq. (10) of Morris (1985), where we assume 4000 K objects measured at 8000 Å for both parameters. For edge-on RG EB twins, $(m_2)/(m_1)\sin^2 i \approx 1$, and thus Eq. (2) reduces to:

$$\Delta M \approx 2.96 \left(\frac{R_1}{a} \right)^3 = 0.024 \left(\frac{R_1/a}{0.2} \right)^3 \quad (3)$$

which corresponds to the typical between-eclipse trends seen in Figs. 3, 4, and 5.

Some readers may be concerned about a possible factor of 2 degeneracy in the period calculation: Devor (2005) assumes there are always two measurable eclipses. We argue that this is a valid assumption for these stars. First, with their position on the bulge CMD and the match between their photometric and orbital radii, we are confident that these are RG stars. Second, the eclipse depths seen in Figs. 3, 4, and 5 range from 0.1 mag to 0.4 mag. It is difficult to conceive of a plausible object that could eclipse $\approx 30\%$ of a RG's light and not be a RG itself, at which point two eclipses would be inevitable.

The third source of error is that of the eclipse phase. Observers may wish to know the phase of the orbit to optimize their RV targeting, for example by obtaining the spectra during the secondary eclipse, when the smaller RG is fully obscured by the larger RG, an epoch we label E_2 . Unfortunately, knowledge of the period phases is now somewhat lost, since OGLE-II observations (Udalski *et al.* 1997, Szymański *et al.* 2005) were taken in the period 1997–2000, and typical periods for these sources is 20 days. Additionally, many of our values of E_2 may be off by $\approx P/2$ if the photometric fit incorrectly determined the surface brightness ratio of the two stars. This phase drift will be easy to account for once time-series photometry from the OGLE-III survey (Szymański *et al.* 2011) become available, as these will allow tighter period determinations and cover the time baseline 2002–2009.

2.2. Biases in the Sample of Devor (2005)

We compare our derived distribution of R_2/R_1 for both the gold and silver samples, shown in panels (a) and (b) of Fig. 2, and we find that these are not consistent

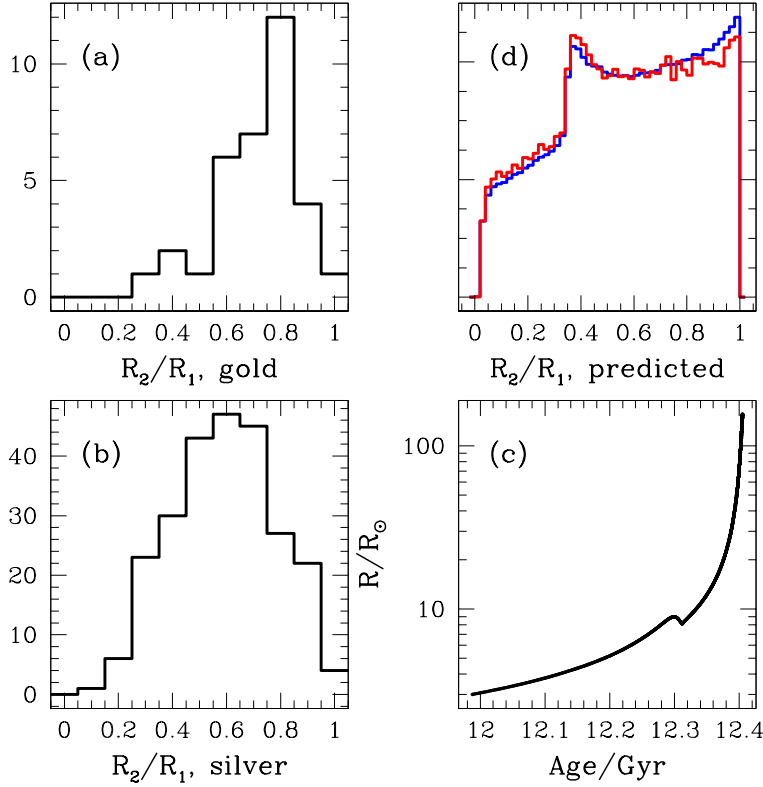


Fig. 2. Observed distribution of R_2/R_1 does not match simple expectations, suggesting selection effects. *Panel (a)*: R_2/R_1 for the 34 gold sample EB systems. *Panel (b)*: R_2/R_1 for the 248 silver sample EB systems. *Panel (c)*: a solar chemistry, $1 M_\odot$ stellar track computed using the Yale Rotating Stellar Evolution Code (YREC, van Saders and Pinsonneault 2012), we show the track for $R \geq 3 R_\odot$, up to the tip of the RG branch. *Panel (d)*: predicted R_2/R_1 for any binary RG twin sampling the probability density function from *Panel c* (blue), and predicted R_2/R_1 for detached binary RG twins modified to account for the period distribution of Duquennoy and Mayor (1991), and assuming an eclipse probability $(R_1 + R_2)/a$ (red).

with expectations: the catalog is likely missing RG EB twins with both high and low radius ratios. The expected probability density functions for R_2/R_1 are derived by sampling a scaled-solar stellar track (Delahaye *et al.* 2010, see Section 3) in the evolution phase during which $R \geq 3 R_\odot$ but before the tip of the RG branch (mimicking our selection for the gold sample). Due to the fact that the mass difference for equal metallicity and co-eval stars on the RG branch is small, it follows from the fuel-consumption theorem (Renzini and Buzzoni 1986) that the relative number counts are simply proportional to the duration of specific phases of stellar evolution, in this case:

$$N(r) dr \propto \tau(r) dr. \quad (4)$$

We randomly sample the stellar track in age (equivalent to sampling in phase) 2×10^6 times, and in panel (d) of Fig. 2 we show (in blue) the resulting distribution of R_2/R_1 . We also show a corrected predicted probability density function (in

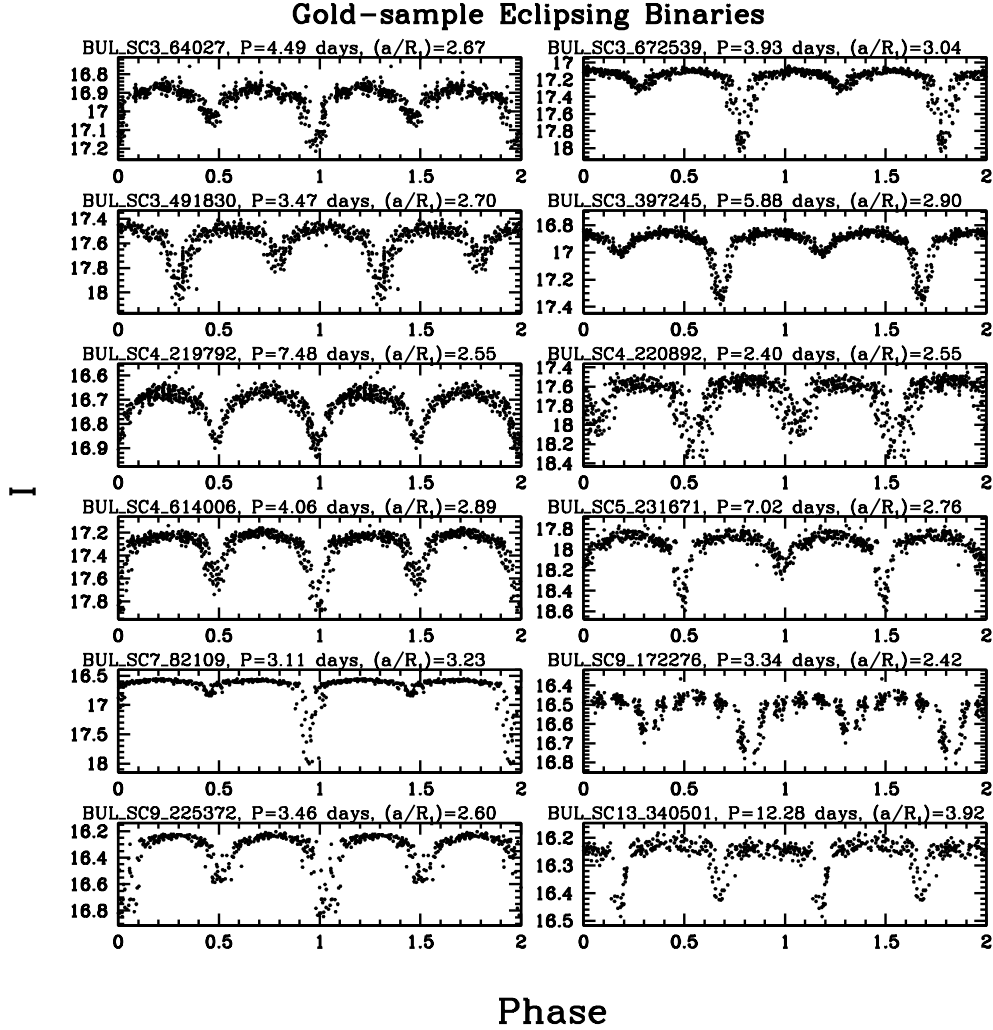


Fig. 3. OGLE-II photometry (Udalski *et al.* 1997, Szymadłowski *et al.* 2005) for gold-sample eclipsing binary stars phase-folded over the periods measured by Devor (2005). For each binary we state the OGLE-II identification, as well as the period and ratio of semimajor axis to primary radius measured by Devor (2005).

red) that accounts for the empirical period distribution of Duquennoy and Mayor (1991) given the assumption that $M_1 = M_2 = 1 M_\odot$, the requirement that the EBs be detached, and the assumption of an eclipse probability $P(E) = (R_1 + R_2)/a$. The ratio of R_2/R_1 is predicted to increase smoothly, approximately doubling, over the range $0 \leq R_2/R_1 \leq 1$, with an excess at $R_2/R_1 \approx 0.45$ due to the red giant branch bump (RGBB). Instead, both the gold and silver sample peak at $R_2/R_1 \approx 0.75$, with a sharp drop-off at both ends.

We suggest two plausible reasons for the difference between the observed and predicted distributions of R_2/R_1 . At low values of R_2/R_1 , the photometric eclipse

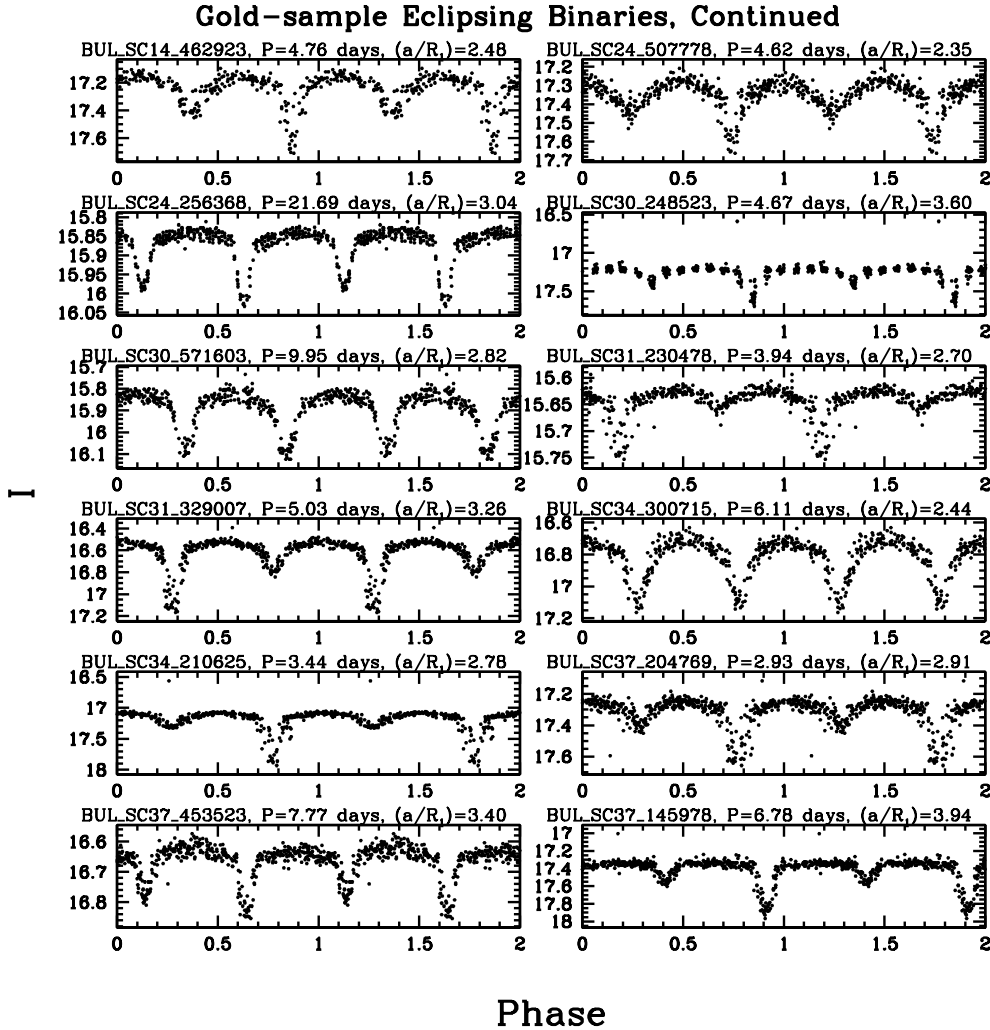


Fig. 4. Same as in Fig. 3.

depth drops rapidly, and thus may evade detection by the algorithm of Devor (2005). At high values of R_2/R_1 , the eclipses may become identical in shape, a solution that may be indirectly biased against by the detection algorithm. We argue against the RC playing a significant role in these biases. It is not included in our predicted luminosity function, but as can be seen in the top left panel of Fig. 1, very few of the EB twins (either gold or silver) are in the RC. There is a sound theoretical reason to expect this. All RC stars will have previously ascended the RG branch and reached very high values of R/R_\odot . Thus, if they have a binary companion sufficiently close as to have detectable eclipse once their size shrinks to $R \approx 10 R_\odot$, they would have significantly overflowed their Roche lobes, and thus likely ended up on a section of the zero-age horizontal branch corresponding to higher mass loss.

Due to the biases in the sample, we cannot assess whether our assay is consis-

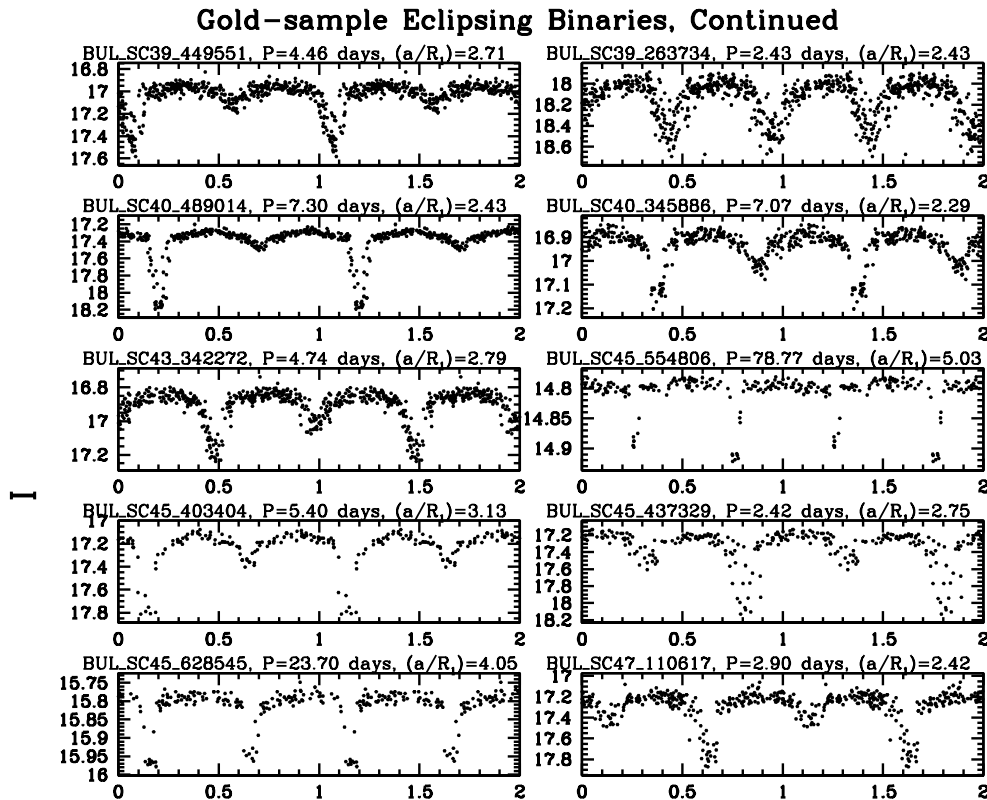


Fig. 5. Same as in Fig. 3.

Phase

tent with the claim that close binaries have a flat secondary mass function, a result observed for various types of binary stars (Kuiper 1935, Pinsonneault and Stanek 1996). If the detection efficiency is far below 100%, then our estimate of 200 “gold” candidates waiting to be found in OGLE-III data is an underestimate. We derived this number by taking the 34 candidates found in OGLE-II and scaling by the ratio (≈ 6) of bulge RR Lyr found in OGLE-III (Soszyd’zski *et al.* 2011) to that found in OGLE-II (Collinge *et al.* 2006). However, if RG EB twins in OGLE-II had a low detection efficiency, the benefit of using the higher-cadence, longer-baseline, and more precise OGLE-III data will be substantially higher than naively estimated.

3. Stellar Models

We use the Yale Rotating Stellar Evolution Code (YREC, van Saders and Pinsonneault 2012) for the theoretical predictions provided in this work. The models

are computed with diffusion. In order to match the observed atmospheric metals-to-hydrogen ratio $Z/X = 0.0229$ (Grevesse and Sauval 1998), solar radius R_{\odot} , and solar luminosity L_{\odot} at $t = 4.57$ Gyr, the models used in this work have the solar composition set to $(Z_{\odot}, Y_{\odot}) = (0.01875, 0.27357)$, and mixing length parameter α of 1.9449.

4. Early Scientific Payoffs of a Spectroscopic Survey of Detached Red Giant Eclipsing Binary Pairs

An early spin off of measurements of the Galactic bulge detached RG eclipsing binary population would be either the validation or invalidation of several predictions derived from the age-helium-metallicity relations assumed and stated in the literature. The mass of RG stars is predicted to have the following functional de-

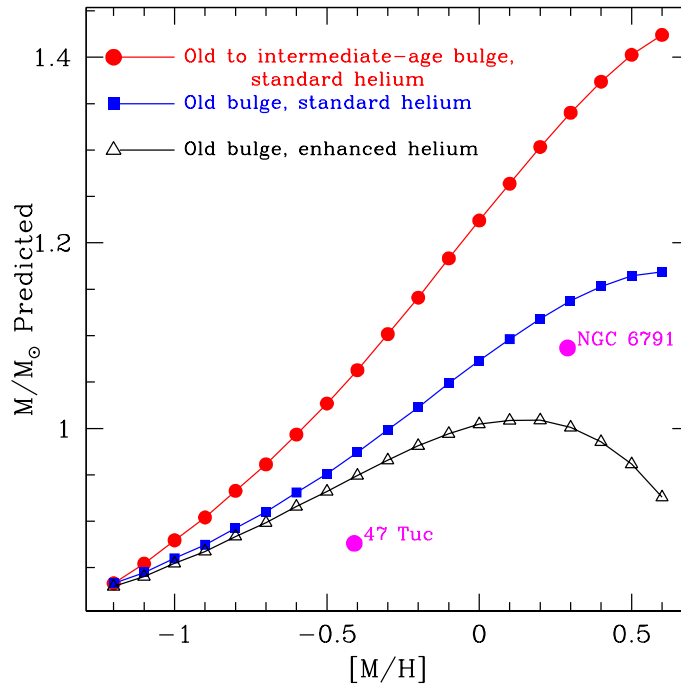


Fig. 6. Different assessments of the age and helium abundance of the bulge predict sharply distinct, easily-measurable RG mass-metallicity relationships. The old stellar population curves (blue, black) are characterized by age-metallicity relations that are linear with $\log(t/10)$ in the range $-1.2 \leq [M/H] \leq +0.6$, $10 \leq t/\text{Gyr} \leq 12$, whereas the old-to-intermediate age curve (red) assumes $5 \leq t/\text{Gyr} \leq 12$ over the same metallicity range. The helium-enhanced curve (black) assumes $\Delta Y/\Delta Z = 3$. We show the approximate turnoff mass (magenta) for the old, (relatively) metal-poor Galactic globular cluster 47 Tuc (Thompson *et al.* 2010), and the approximate turnoff mass for the old, metal-rich open cluster NGC 6791 (Brogaard *et al.* 2011). Both EBs shown in magenta are near the turnoff, and thus expected to have masses slightly lower ($\Delta M \approx 0.1 M_{\odot}$) than that on the RG branch.

pendence on metallicity, age and initial helium abundance:

$$\log \left(\frac{M}{M_{\odot}} \right)_{\rho=-3.0} = 0.026 + 0.126 \left[\frac{M}{H} \right] - 0.276 \log \left(\frac{t}{10} \right) - 0.937(Y - 0.27), \quad (5)$$

and thus specific claims about the bulge age-helium-metallicity relation derived from its CMD morphology predict equally specific mass-metallicity relations for bulge RG stars. Fig. 6 shows that the mass-metallicity relations predicted are very distinct. For example, Bensby *et al.* (2011) assume isochrones with a standard helium-to-metals enrichment ratio and find that stars with $[\text{Fe}/\text{H}] = +0.35$ have an age of ≈ 6 Gyr. If true, RGs at that metallicity should have masses of $\approx 1.35 M_{\odot}$. If this is the typical mass found for that metallicity it would confirm their interpretation, and would invalidate the hypothesis that the entire bulge stellar population formed by rapid gravitational in-fall, an invalidation already suggested by dynamical investigations of metal-rich M-giants (Shen *et al.* 2010, Kunder *et al.* 2011). Alternatively, if the bulge is enhanced in helium, as argued based on measurements of the bulge red giant branch bump (Nataf *et al.* 2011a,b) and the discrepancy between spectroscopic and photometric turnoff ages (Nataf and Gould, 2011), then RG masses should be significantly lower. If $(\Delta Y/\Delta Z)_{\text{bulge}} = 3$ and the population is older than $t = 10$ Gyr, no masses greater than $\approx 1 M_{\odot}$ should be measured on the RG branch.

The combination of RG mass and metallicity measurements with MSTO single-star spectroscopic measurements is enough to determine both the age-metallicity and helium-metallicity relationships of the bulge. Eq. (5) shows that at fixed metallicity, increased age has the same effect as increased Y : both lead to decreased mass. This degeneracy has the opposite angle to that found on the MSTO and sub-giant branch (SGB): increased Y behaves similarly to decreased age, as both lead to higher temperatures on the MSTO and lower surface gravities on the SGB (Nataf and Gould 2011).

There could also be a strong metallicity dependence to the binary fraction. Would the RG eclipsing binary metallicity-distribution function (MDF) match that of the measured bulge RG MDF? If binaries are not a representative sample of the underlying population, a significant fraction of the bulge stellar population might not be directly probeable by this method. This would be interesting in its own right, as it could constrain models of how stars form in environments with different metallicity, an issue recently brought into sharper focus by Conroy and van Dokkum (2011). Moreover, there would still be value in measuring the age and helium abundance of the bulge within the remaining metallicity range.

These stars would also be powerful dynamical probes. As these are bright stars, their OGLE-III proper motions will be very precise. Their physical radii would measure where these stars are located in the bulge relative to the RC. This would give the distance, and would enable conversion of proper motions into transverse velocities. The dynamics of the bulge are known to be complex, with an X-shape

at large separations ($Z \geq 500$ pc) from the plane recently discovered (Nataf *et al.* 2010, McWilliam and Zoccali 2010), and correlations between kinematics and metallicity at all latitudes (Babusiaux *et al.* 2010). A stellar sample with six measured kinematic phase space coordinates is needed.

Mass loss along the RG branch is another scientific prospect. Brown *et al.* (2011) found a significant number of low-mass white dwarfs without binary companions, implying that a significant number of stars skip stages of post-main-sequence stellar evolution, possibly due to enhanced mass loss in metal-rich stars. This would be consistent with the spectroscopic study of Rich *et al.* (2011), which showed that the $[\text{Fe}/\text{H}] \approx +0.35$ peak detected among bulge dwarf and SGB stars (Bensby *et al.* 2010, 2011) is not present among bulge M-giants. Significant mass loss would manifest itself as a much lower mass for more luminous stars, a characteristic that could easily be measured in a sufficiently large survey.

5. Population Parameters and Observables

The observable properties of a RG in an eclipsing binary pair are mass, density, metallicity, and effective temperature. These four observables can be matched to three theoretical quantities that effectively determine the initial state of the star (mass, helium, and metallicity), plus the evolutionary state at which we evaluate the stellar track. In principle, this match between the number of independent parameters and measurements enables complete determination of the age and helium abundance of each detached RG eclipsing binary pair. For the purposes of this section, we ignore theoretical uncertainties in the temperature and metallicity scale, and discuss what can be done if one assumes accurate stellar models and maximum-likelihood measurements and errors of the observables. We base our parametrization on $\log \rho$ rather than $\log g$ because the density, derived by plugging the EB light curve parameters into Kepler's 3rd law, is typically measured with substantially higher accuracy than the surface gravity.

Before moving forward, we must recognize that the accuracy of RG temperature estimates as well as the interpretive power thereof is a matter of ongoing controversy. There remains a ≈ 100 K uncertainty in the temperature determination of stars (Casagrande *et al.* 2010), and this uncertainty is comparable in size to the predicted effects of large age or helium variations. Moreover, for the sample of close binaries listed in this work, $(R_{1,2}/a) \approx 0.2$, and thus star-star interactions may have a significant impact on the observed stellar properties (Chabrier *et al.* 2007). Additionally, the convective efficiency assumed in this work, parametrized by the mixing length, is calibrated on the Sun, and there is no *a priori* reason why the efficiency should be the same in RGs. However, there remains value in working out the standard theoretical predictions, which may still be very effective for the most well-detached systems. The prospects of calibrating the zero-point terms for RG relationships are decent, due to the information accessible with missions such

as Kepler (*e.g.*, Hekker *et al.* 2010, 2011, Miglio *et al.* 2012). Additionally, whereas the interpretation of T_{eff} should be significantly impacted by these concerns, that of M/M_{\odot} should not – the mass observed in the RG phase is almost entirely a function of the main-sequence lifetime for a given initial mass, metallicity and helium abundance. Any EB with star-star interactions in the RG phase will not have experienced such interactions during the main-sequence, as $R_{1,2}/a$ will have been several times smaller.

Facilitating the task of parameter estimation is the fact that the observable properties are predicted to be linear or nearly linear in the parameter range of interest: stars of intermediate age and older. We use our library of stellar tracks to derive relationships for the parameter range $-3.5 \leq \log(\rho/\rho_{\odot}) \leq -2.5$, $-0.40 \leq [\text{M}/\text{H}] \leq 0.40$, $5 \leq t \leq 15$ Gyr, $0.25 \leq Y \leq 0.40$:

$$D_i = \kappa_{ij}\eta_j + D_{i0} \quad (6)$$

where

$$D_i = \begin{pmatrix} Y \\ \log(t/10) \end{pmatrix}, \quad \eta_j = \begin{pmatrix} \log(T_{\text{eff}}) - 3.65 \\ [\text{M}/\text{H}] \\ \log(\rho/\rho_{\odot}) + 3 \\ \log(M/M_{\odot}) \end{pmatrix}, \quad (7)$$

and

$$\kappa_{ij} = \frac{\partial D_i}{\partial \eta_j} = \begin{pmatrix} 7.1208 & 0.28426 & -0.21878 & -0.50889 \\ -24.176 & -0.51046 & 0.7387 & -1.8901 \end{pmatrix}, \quad D_{i0} = \begin{pmatrix} 0.26516 \\ 0.10957 \end{pmatrix}. \quad (8)$$

The errors and covariance matrix in $D_i = (Y, \log(t/10))$ are given by

$$\sigma_i = \sqrt{C_{ii}}, \quad C_{ij} = \sum_{m,n=1}^4 \kappa_{im}\kappa_{jn}c_{mn} \quad (9)$$

where c_{ij} is the covariance matrix of the observables.

Eq. (8) again emphasizes the crucial role of a mass measurement. Note that a change in any of the first three quantities ($\log T_{\text{eff}}$, $[\text{Fe}/\text{H}]$, $\log \rho$) induces motions of Y and $\log t$ in opposite directions, while a change in $\log M$ induces motion in the same direction. Therefore, without a tight mass measurement it is impossible to jointly constrain the helium content and age of the star. This is illustrated graphically in Figs. 7 and 8.

Fig. 7a shows the age-mass relation for RG stars at solar metallicity for different helium abundances. Note that the curves are both straight and equally spaced, *i.e.*, a linear relation. This implies that perfect mass and metallicity measurements would yield a 1-dimensional linear constraint on the $Y - \log(t/10)$ plane. In fact, while an essentially perfect mass measurement is quite feasible (see below), this is not so for metallicity, as such the 1-dimensional constraint would be a band rather than a line.

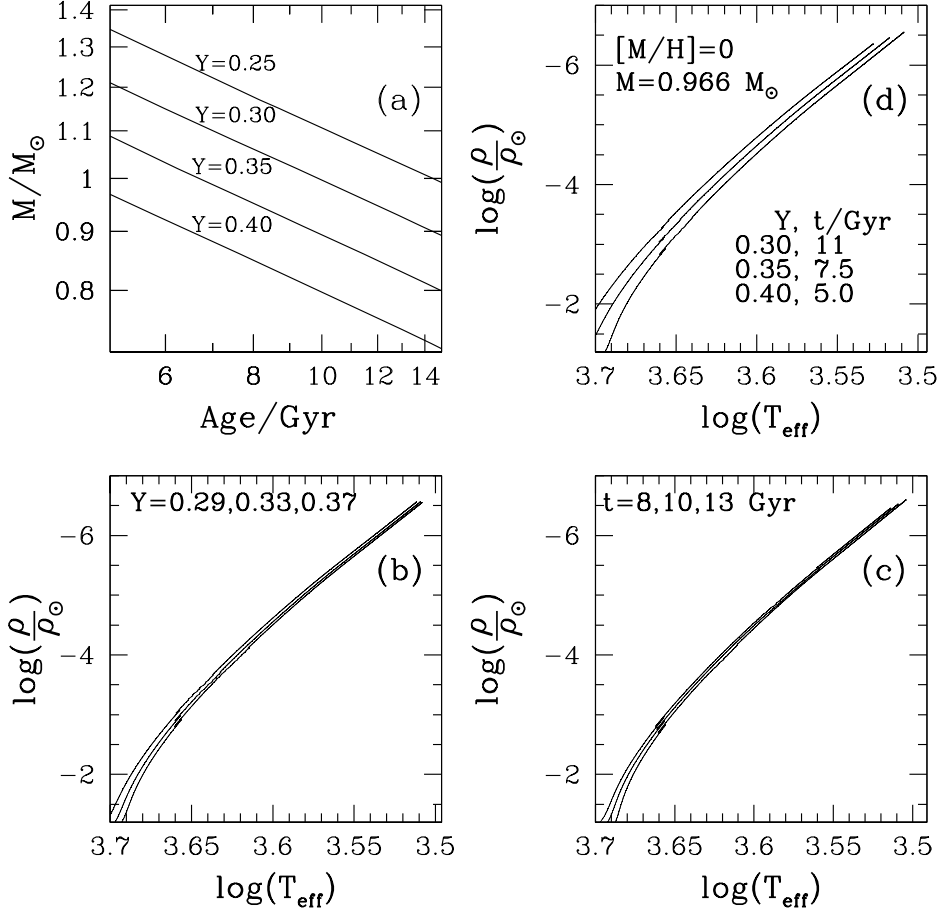


Fig. 7. Predicted relationships between RG parameters and observables. *Panel (a)*: M/M_{\odot} as a function of age for $[M/H]=0$ tracks varying in initial helium. Lower mass means higher age or higher helium. *Panel (b)*: RG tracks with $[M/H]=0$, $t=11$ Gyr varying in initial helium. Higher helium at fixed metallicity and density implies a hotter RG branch. *Panel (c)*: RG tracks with solar chemistry varying in age. Higher age at fixed chemistry and density implies a colder RG branch. *Panel (d)*: these two effects add constructively when the mass is fixed, because age goes down as helium abundance goes up.

This band is almost perfectly orthogonal to the constraint that can be obtained from spectroscopy ($\log T_{\text{eff}}$, $[\text{Fe}/\text{H}]$, $\log g$), which is shown in Fig. 8. Like the mass/metallicity constraint, spectroscopy by itself measures one fewer quantity than the number of model parameters being constrained, and thus is represented by parallel-line error contours, rather than closed contours. For purposes of this and subsequent plots, we begin with the covariance matrix $c_{ij} = e_i e_j \text{cor}_{ij}$, of a typical RG star (from Alves-Brito *et al.* 2010)

$$e_j = \begin{pmatrix} \sigma_{\log T_{\text{eff}}} \\ \sigma_{[\text{M}/\text{H}]} \\ \sigma_{\log g} \end{pmatrix} = \begin{pmatrix} 0.0044 \\ 0.161 \\ 0.184 \end{pmatrix}, \quad \text{cor}_{ij} = \begin{pmatrix} 1 & 0.36 & 0.39 \\ 0.36 & 1 & -0.64 \\ 0.39 & -0.64 & 1 \end{pmatrix} \quad (10)$$

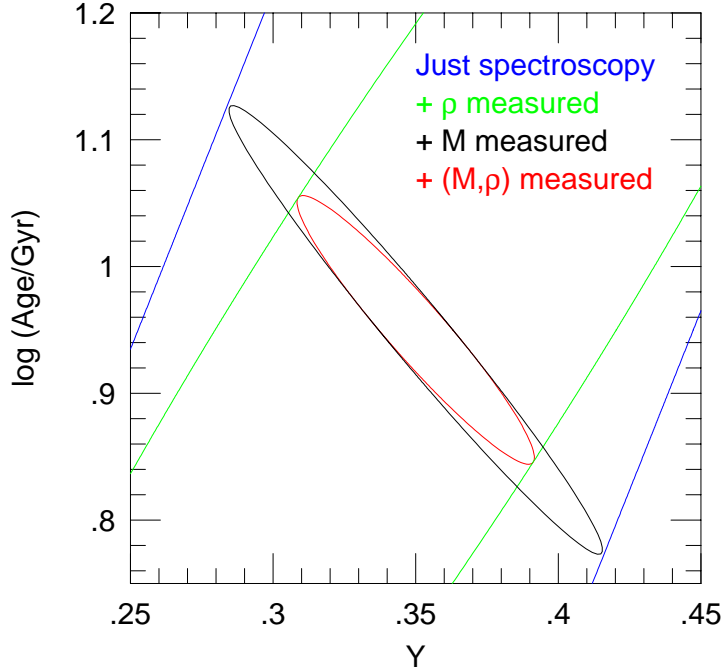


Fig. 8. Predicted constraints on the age-helium plane from spectroscopy only ($\log T_{\text{eff}}, [\text{Fe}/\text{H}], \log g$) (blue), spectroscopy plus density measurement (green), spectroscopy plus mass measurement (black), and all measurements (red), assuming measured properties ($M/M_{\odot}, [\text{M}/\text{H}], T_{\text{eff}}, \log(\rho/\rho_{\odot}) + 3$) = $(0.91 \pm 0.01, 0.0 \pm 0.1, 4563 \pm 30, 0 \pm 0.01)$. With just spectroscopy, age and helium are completely degenerate. Even precise measurement of the density only narrows this degeneracy, it does not effectively break it. On the other hand, a mass measurement generates an orthogonal constraint on this plane and so does, by itself, break the degeneracy. Combining mass and density measurements then further reduces the errors by a factor 1.6.

which has been derived directly from the ensemble of line measurements, using the method of Epstein *et al.* (2010). We then multiply the errors by a factor $2/3$, in recognition of the fact that the mass measurements will require multiple epochs of high S/N, high-resolution spectra.

We now turn to the impact of a ρ measurement, first combined only with spectroscopy (Eq. 10) and then with a mass measurement as well. Unlike mass and metallicity, the other three quantities that one can hope to directly measure ($\log T_{\text{eff}}, \log \rho, \log g$) all depend strongly on phase of stellar evolution. In Fig. 7bc, we show these tracks on the $\log T_{\text{eff}}/\log \rho$ plane for various values of Y and $\log(t)$ respectively. The main point to take away from these panels is that even if the age (panel b) or the helium content (panel c) were known exactly, it would be very difficult to distinguish the tracks from precise temperature and density measurements. Only if the mass is measured, so these two effects can be combined, do the tracks become well-separated (panel d).

The impact of a density measurement (combined with spectroscopy) on the age-helium plane is shown by the green curves in Fig. 8. Like the spectroscopy-only

constraint (blue), these appear to be parallel lines, which is surprising given that there are four measurements ($\log T_{\text{eff}}$, $[\text{Fe}/\text{H}]$, $\log g$, $\log \rho$) to constrain four model parameters. In fact, these contours are part of an ellipse which is extremely elongated in the direction orthogonal to the mass constraint. The reason for this is essentially the same as spectroscopy-only case: weak coupling of $\log M$ to Y and $\log t$ via error propagation from the $\log g$ measurement. Fig. 8 also shows the impact of adding a mass measurement to either of these cases. When all measurements are combined, the error ellipse is highly elongated along the direction of the mass constraint, with its width essentially determined by the metallicity error. Note the $\log M$ and $\log \rho$ measurements have both been assumed to have errors of 0.01 dex (2.3%). However, this diagram would look almost exactly the same if we had assumed zero errors for both quantities. Hence, even conservative error bars are equivalent to perfect measurements for the $\log M$ and $\log \rho$. We note that the detached RG EB twins OGLE SC10 137844, whose parameters are somewhat more difficult to measure due to the fact they are in a highly eccentric ($e = 0.31$) and long-period system ($P = 372$ days), recently had their masses measured to $\approx 0.8\%$ and densities to $\approx 4.5\%$ (Graczyk *et al.* 2012).

The actual spectroscopic measurements would be greatly constrained by the eclipsing binary light curve. Aside from the precisely measured values of $\log g$ obtained from $\log \rho$ and M/M_{\odot} , relative temperatures and luminosities would be known to a high degree of accuracy from the photometry alone, reducing the degrees of freedom allowed in the spectroscopic fit. That the two stars are in a moderately close binary would strongly suggest that they have identical metallicities. Further, the ability to take spectra during eclipse, when only the larger and thus brighter star would contribute to the spectrum, guarantees spectroscopic parameters at least as good as those of a single RG. We note that for these systems the eclipses often last several days, making the acquisition of single-star spectra very feasible. We also comment on an important recent finding. Gonzalez *et al.* (2011ab) used dereddened near-IR photometry of the Galactic bulge and showed that the photometric color distribution of bulge stars was in itself sufficient to reproduce the spectroscopic bulge metallicity distribution function. This demonstrates that the bulge RG temperatures are well-behaved.

6. Discussion

6.1. The Effect of Uncertainties in Stellar Evolution Models

The stellar models that are used to interpret the measurements are themselves a source of uncertainty. Heavy element diffusion, the value of the mixing length, and angular momentum evolution are among the uncertainties of stellar evolution. Whereas mass and metallicity measurements should yield immediate and powerful constraining power, temperature measurements will be more difficult to interpret due to their greater theoretical uncertainties. This is due to the fact that stellar

models are typically calibrated with respect to the Sun, a main-sequence star. Thus main-sequence behavior (*e.g.*, main-sequence lifetime as a function of mass and composition) is better calibrated than post-main-sequence behavior. Interpreting RG temperatures will therefore require greater care than interpreting masses. There will be at least three different means to constrain the impact of these uncertainties.

We ran several models with varied input parameters to gauge the effect of two of the most significant uncertainties: the mixing length and diffusion. Reducing the mixing length to 1.6449 from 1.9449, a shift comparable in size to the empirical (Ferraro *et al.* 2006) and theoretical (Trampedach and Stein 2011) determinations of the uncertainty, has the effect of increasing the stellar lifetime at fixed mass, metallicity and helium by $\approx 1\%$ – the effect is negligible. For diffusion, we computed the same models without diffusion, an exaggeration of the size of the error in diffusion, and these yielded a stellar lifetime decrease of $\approx 3\%$. Note that turning off diffusion requires small changes in the metals abundance and the mixing length to maintain consistency with the solar constraints, see Table 1 of van Saders and Pinsonneault (2012). Both effects are smaller than the statistical error resulting from a typical precision in the metallicity of ≈ 0.1 dex. We also verified that the mass predictions for RG stars in this work agree with those of the BaSTI (Pietrinferni *et al.* 2006) and Dartmouth (Dotter *et al.* 2008) stellar databases – agreement is to $\approx 1\%$ on the lower RGB.

An excellent way to constrain the effect of theoretical uncertainties would be to exploit the fact that the relative predictions of stellar evolution models are more reliable than the absolute predictions. A reasonable choice for an anchor point would be requiring the most metal-poor stars to have the same age as the Galactic globular clusters (GCs), $t_{GC} = 12.8 \pm 0.4$ Gyr (Marín-Franch *et al.* 2009), and to have a primordial helium abundance for those stars of $Y = 0.249$ (Simha and Steigman 2008). In principle, the metal-poor bulge may in fact be a little older: bulge RR Lyr stars are more metal-rich than those in globular clusters (Kunder and Chaboyer 2008, Pietrukowicz *et al.* 2011), which might imply that the most metal-poor bulge stars are too old to generate many RR Lyrae stars. However, since the age difference between the GCs and the universe is not large, such a difference would not significantly undermine the use of the GCs as an age anchor point.

At Disk-like metallicities (*i.e.*, $[\text{Fe}/\text{H}] \approx -0.3$), there is a campaign to measure precise abundances of RG stars that have asteroseismic measurements from the KEPLER and COROT satellites (Epstein *et al.* 2010, NOAO-2011A-0510). Due to the fact that these are Disk stars, which are expected to have younger ages and likely different helium-enrichment patterns, we should expect that the $\log g - T_{\text{eff}} - [\text{M}/\text{H}]$ mapping will not be identical to the mapping that can be obtained for bulge stars. It will be interesting to see how they differ. The differences would be combined with the predictions of Eq. (8) to yield estimates of the relative age and helium offsets between these two stellar populations.

At the metal-rich end, the open cluster NGC 6791 is a potent anchor. It has a

high metallicity $[\text{Fe}/\text{H}] = +0.40$, it is the subject of detailed asteroseismic study from Kepler photometry (Miglio *et al.* 2012), and has three eclipsing binary pairs with measured masses and radii including two near the main-sequence turnoff (Grundahl *et al.* 2008, Brogaard *et al.* 2011). An interesting finding of Miglio *et al.* (2012) is that the mass loss for the metal-rich RG stars in NGC 6791 is not large: $\Delta\bar{M} \approx 0.09 M_{\odot}$. However, this finding is suggestive rather than conclusive due to the use of first-order asteroseismic scaling relations, which are still a matter of ongoing investigation. A direct mass measurement of mass loss would be helpful, and this could be detected if it were found that RG stars at the same metallicity have a luminosity-dependent mass. With enough luck, one or several EBs at large periods may even be found on the RC phase of stellar evolution. Short-period EBs with RC members would not be adequate, as it is likely that these detached EBs would not have been detached when the RC was a much larger upper-RG branch star.

The combined use of these three anchors and the relative predictions of stellar evolution could over determine the properties of bulge stars. Because they span the entire metallicity range $-1.2 \leq [\text{M}/\text{H}] \leq +0.60$ (Zoccali *et al.* 2008, Johnson *et al.* 2011, Hill *et al.* 2011), any residual uncertainty could be used to place bounds on the uncertainties in stellar models.

6.2. Other Uncertainties

There are several systematic effects that could pose challenges to any survey of eclipsing binary pairs. We show, however, that these could either be controlled or become investigative avenues in their own right.

The first is that blending can affect the light curve of bulge eclipsing binaries, a systematic that is not generally a concern in the solar neighborhood. The extra flux from a blend, F_b , would bias the interpretation of the flux drop during the eclipse, and thus the value of the derived stellar density. In Appendix, we derive that:

$$\Delta \ln \rho_1 = -\frac{3 F_b}{4 F_1}. \quad (11)$$

It follows from Eqs. (6) and (11) that a 10% blend would significantly affect the derived stellar parameter values. This could be controlled by getting high-resolution images of the target in *JHK*. A significant blend could also be estimated from its contribution to the spectra, as its spectral lines would not share the ≈ 100 km/s orbital velocities. Thus, it likely that the blending fraction F_b/F_1 could be measured to a precision of a few percent.

The second effect is the RGBB. This post-main-sequence phase of stellar evolution, during which the star temporarily gets fainter, before getting brighter again (Cassisi and Salaris 1997, Bjork and Chaboyer 2006, Nataf *et al.* 2011b), breaks the injective mapping between density and temperature at fixed mass, helium and metallicity. The resulting difference in temperature can yield an offset in the derived values of $\delta Y \approx 0.007$ and $\delta \log(t/10) \approx 0.02$. However, this would only

occur at the position of the RGBB, which can be easily estimated to a precision of ≈ 0.04 dex in $\log g$ (*i.e.*, ≈ 0.1 mag) as its characteristic luminosity and number counts are steep, empirically-calibrated functions of metallicity (Nataf *et al.* 2011b). The lifetime of the RGBB for bulge stars (≈ 20 Myr, Nataf *et al.* 2011a) does not contribute to the total age uncertainty, as independent errors add in quadrature, and that of the metallicity determination would dominate.

The third issue is that of RS Canum Venaticorum (RS CVn) type stars (Eaton and Hall 1979). These heavily spotted systems, common in binaries, would have effective temperatures distinct from those predicted by naive models. If close-in binaries were found to have lower temperatures at fixed density and metallicity, this would demonstrate an effect due to tides and angular momentum transfer. The superior photometry from OGLE-III, with its greater cadence, longer baseline, and higher precision, should impose upper bounds on the spot depth of eclipsing binary candidates, which could be further investigated by measuring the calcium H+K emission in the spectra. We note that identification of RS CVn could be a good way to identify binaries that are not RG-EB twins, which would be a means of expanding the sample.

Stellar rotation could also be a concern. While isolated solar-mass stars tend to spin down over time, their cousins in binary systems are tidally circularized after 7 Gyr for periods $P < 15$ days and after 12 Gyr for periods $P < 20$ days (Mathieu *et al.* 2004). Although tidal synchronization is not the same as circularization, the two are closely related. Thus, at least the closer RG eclipsing systems were probably rotating faster than the Sun ($P = 25$ day) while they were on the main sequence. Sills *et al.* (2000) showed that at fixed mass and composition, RG stars whose progenitors were rotating with periods $P = 8$ day are predicted to be slightly colder than non-rotating RG stars yielding an estimated systematic effect of $\Delta Y \approx 0.01$. Since the RG eclipsing binaries are at longer periods, the effect will be even smaller, but should nevertheless be taken into account.

7. Conclusion

We have demonstrated that there are observable, detached RG eclipsing binary pairs in the Galactic bulge, and have constructed gold and silver samples of 34 and 248 candidates respectively by imposing strict physical consistency requirements on the total OGLE-II eclipsing binary sample of Devor (2005). We have demonstrated that the derived masses, temperatures, metallicities and densities assuming reasonable error estimates would give powerful constraints on the formation and evolution of the Galaxy: both the age and helium abundance would be tightly constrained, at every measured metallicity. In addition to providing fundamental insights on Milky Way assembly, a survey of these systems would have the potential to teach us about the metallicity-dependence of the binary fraction, mass loss on the RG branch and stellar models. Our count of 34-(282) such systems in the OGLE-II

eclipsing binary catalog leads us to estimate that at least 200-(1500) could be found in OGLE-III, just from the larger viewing area.

Acknowledgements. DMN was primarily supported by the NSERC grant PGSD3-403304-2011. DMN and AG were partially supported by the NSF grant AST-1103471. MHP was partially supported by NASA grant NNX11AE04G. We thank Jan Skowron, Jason Eastman, Francis Fekel and Martin Asplund for helpful discussions.

REFERENCES

- Al-Naimiy, H.M. 1978, *Astrophys. and Space Sci.*, **53**, 181.
 Alves-Brito, A., Meléndez, J., Asplund, M., Ramírez, I., and Yong, D. 2010, *A&A*, **513**, A35.
 Assef, R.J., *et al.* 2006, *ApJ*, **649**, 954.
 Babusiaux, C., *et al.* 2010, *A&A*, **519**, A77.
 Bensby, T., *et al.* 2010, *A&A*, **512**, A41.
 Bensby, T., *et al.* 2011, *A&A*, **533**, A134.
 Bessell, M.S., and Brett, J.M. 1988, *PASP*, **100**, 1134.
 Bjork, S.R., and Chaboyer, B. 2006, *ApJ*, **641**, 1102.
 Brogaard, K., *et al.* 2011, *A&A*, **525**, 2.
 Brown, J.M., Kilic, M., Brown, W.R., and Kenyon, S.J. 2011, *ApJ*, **730**, 67.
 Casagrande, L., Ramírez, I., Meléndez, J., Bessell, M., and Asplund, M. 2010, *A&A*, **512**, A54.
 Cassisi, S., and Salaris, M. 1997, *MNRAS*, **285**, 593.
 Chabrier, G., Gallardo, J., and Baraffe, I. 2007, *A&A*, **472**, L17.
 Clarkson, W.I., *et al.* 2011, *ApJ*, **735**, 37.
 Collinge, M.J., Sumi, T., and Fabrycky, D. 2006, *ApJ*, **651**, 197.
 Conroy, C., and van Dokkum, P. 2011, arXiv:1109.0007.
 Delahaye, F., Pinsonneault, M.H., Pinsonneault, L., and Zeppen, C.J. 2010, arXiv:1005.0423.
 Devor, J. 2005, *ApJ*, **628**, 411.
 Dotter, A., *et al.* 2008, *ApJS*, **178**, 89.
 Duquennoy, A., and Mayor, M. 1991, *A&A*, **248**, 485.
 Eaton, J.A., and Hall, D.S. 1979, *ApJ*, **227**, 907.
 Epstein, C.R., *et al.* 2010, *ApJ*, **709**, 447.
 Epstein, C.R., Johnson, J.A., Pinsonneault, M.H., and Lai, David 2010, NOAO-2011A-0510.
 Ferraro, F.R., Valenti, E., Straniero, O., and Origlia, L. 2006, *ApJ*, **642**, 225.
 Fulbright, J.P., McWilliam, A., and Rich, R.M. 2006, *ApJ*, **636**, 821.
 Gonzalez, O.A., *et al.* 2011a, *A&A*, **530**, A54.
 Gonzalez, O.A., Rejkuba, M., Zoccali, M., Valenti, E., and Minniti, D. 2011b, *A&A*, **534**, A3.
 Graczyk, D., *et al.* 2012, arXiv:1203.2517.
 Grevesse, N., and Sauval, A.J. 1998, *Space Science Reviews*, **85**, 161.
 Grundahl, F., Clausen, J.V., Hardis, S., and Frandsen, S. 2008, *A&A*, **492**, 171.
 Hekker, S., *et al.* 2010, *ApJ*, **713**, L187.
 Hekker, S., *et al.* 2011, *MNRAS*, **414**, 2594.
 Hill, V., *et al.* 2011, *A&A*, **534**, A80.
 Johnson, C.I., Rich, R.M., Fulbright, J.P., Valenti, E., and McWilliam, A. 2011, *ApJ*, **732**, 108.
 Kervella, P., Thévenin, F., Di Folco, E., and Ségransan, D. 2004, *A&A*, **426**, 297.
 Kuiper, G.P. 1935, *PASP*, **47**, 15.
 Kunder, A., and Chaboyer, B. 2008, *AJ*, **136**, 2441.
 Kunder, A., *et al.* 2011, arXiv:1112.1955.
 Lucy, L.B. 1967, *Zeitschrift für Astrophysik*, **65**, 89.

- Marín-Franch, A., *et al.* 2009, *ApJ*, **694**, 1498.
- Marín-Franch, A., Cassisi, S., Aparicio, A., and Pietrinferni, A. 2010, *ApJ*, **714**, 1072.
- Martins, F., *et al.* 2008, *ApJ*, **672**, L119.
- Mathieu, R.D., Meibom, S., and Dolan, C.J. 2004, *ApJ*, **602**, L121.
- McWilliam, A., and Zoccali, M. 2010, *ApJ*, **724**, 1491.
- Miglio, A., *et al.* 2012, *MNRAS*, **419**, 2077.
- Morris, S.L. 1985, *ApJ*, **295**, 143.
- Nataf, D.M., Stanek, K.Z., and Bakos, G.A. 2009, *Acta Astron.*, **59**, 255.
- Nataf, D.M., Udalski, A., Gould, A., Fouqué, P., and Stanek, K.Z. 2010, *ApJ*, **721**, L28.
- Nataf, D.M., Stanek, K.Z., and Bakos, G.Á. 2010, *Acta Astron.*, **60**, 261.
- Nataf, D.M., Udalski, A., Gould, A., and Pinsonneault, M.H. 2011, *ApJ*, **730**, 118.
- Nataf, D.M., Gould, A.P., Pinsonneault, M.H., and Udalski, A. 2011, arXiv:1109.2118.
- Nataf, D.M., and Gould, A.P. 2011, arXiv:1112.1072.
- Pasquini, L., Mauas, P., Käufel, H.U., and Cacciari, C. 2011, *A&A*, **531**, A35.
- Pietrinferni, A., Cassisi, S., Salaris, M., and Castelli, F. 2004, *ApJ*, **612**, 168.
- Pietrukowicz, P., Udalski, A., Soszynski, I., *et al.* 2011, *ApJ*, in press, arXiv:1107.3152.
- Pinsonneault, M.H., and Stanek, K.Z. 2006, *ApJ*, **639**, L67.
- Pribulla, T., and Rucinski, S.M. 2006, *AJ*, **131**, 2986.
- Renzini, A., and Buzzoni, A. 1986, *Spectral Evolution of Galaxies*, **122**, 195.
- Rich, R.M., Origlia, L., and Valenti, E. 2011, arXiv:1112.0306.
- Salpeter, E.E. 1955, *ApJ*, **121**, 161.
- Shen, J., *et al.* 2010, *ApJ*, **720**, L72.
- Sills, A., Pinsonneault, M.H., and Terndrup, D.M. 2000, *ApJ*, **534**, 335.
- Simha, V., and Steigman, G. 2008, *Journal of Cosmology and Astroparticle Physics*, **8**, 11.
- Soszydźski, I., *et al.* 2011, *Acta Astron.*, **61**, 1.
- Szymadźski, M.K. 2005, *Acta Astron.*, **55**, 43.
- Szymadźski, M.K., *et al.* 2011, *Acta Astron.*, **61**, 83.
- Thompson, I.B., *et al.* 2010, *AJ*, **139**, 329.
- Tokovinin, A., Thomas, S., Sterzik, M., and Udry, S. 2006, *A&A*, **450**, 681.
- Trampedach, R., and Stein, R.F. 2011, *ApJ*, **731**, 78.
- Udalski, A., Kubiak, M., and Szymadźski, M. 1997, *Acta Astron.*, **47**, 319.
- van Saders, J.L., and Pinsonneault, M.H. 2012, *ApJ*, **746**, 16.
- Zoccali, M., *et al.* 2008, *A&A*, **486**, 177.

Appendix

Effect of Blending on Derived Eclipsing Binary Parameters

We derive the error made in estimating the densities of the binary components made by failing to detect (and so take into account) blending by a third star within the PSF. For this purpose, we make the simplifying assumptions of uniform surface brightness and highly unequal source sizes. If these assumptions are relaxed, the derivation becomes much more complicated, but the final results are similar.

Define

$$\tau_1 \equiv \pi \frac{t_1}{P} \quad \tau_2 \equiv \pi \frac{t_2}{P}, \quad z_1 \equiv \frac{r_1}{a}, \quad z_2 \equiv \frac{r_2}{a}$$

where t_1 is the transit time, t_2 is the ingress time, P is the period, a is the semimajor axis, and r_1 and r_2 are the two radii. Note that t_i and P can be measured with essentially infinite precision, because they depend only on timing data, and not on blending. Hence, τ_i are also observables with quasi-infinite precision. Then, for circular orbits,

$$\tau_1 = z_1(1 - \beta^2)^{1/2} \quad \tau_2 = z_2(1 - \beta^2)^{-1/2}$$

where β is the impact parameter. Hence, the precision of

$$\beta = \sqrt{1 - \frac{\tau_1 z_2}{\tau_2 z_1}} = \sqrt{1 - \frac{t_1 r_2}{t_2 r_1}} \quad z_1 z_2 = \tau_1 \tau_2$$

depends directly on how well the ratio of radii, r_2/r_1 can be measured. The fluxes in and out of eclipse are related to the two surface brightnesses by

$$F_1 = \pi S_1 r_1^2, \quad F_2 = \pi[S_1(r_1^2 - r_2^2) + S_2 r_2^2] = F_1 + \pi(S_2 - S_1)r_2^2 \quad F_3 = F_1 + \pi S_2 r_2^2$$

Hence,

$$\frac{F_2 - F_1}{F_3 - F_1} = 1 - \frac{S_1}{S_2} \Rightarrow \frac{S_1}{S_2} = \frac{F_3 - F_2}{F_3 - F_1}$$

$$\frac{F_3 - F_1}{F_1} = \frac{S_2 r_2^2}{S_1 r_1^2} \Rightarrow \frac{r_2^2}{r_1^2} = \frac{F_3 - F_2}{F_1} \Rightarrow \eta \equiv \frac{z_2}{z_1} = \frac{r_2}{r_1} = \sqrt{\frac{F_3 - F_2}{F_1}}$$

where $\eta \equiv z_2/z_1$. The inverse density of the whole system is given

$$\frac{1}{\rho} = \frac{4\pi}{3} \frac{r_1^3 + r_2^3}{M} = \frac{4\pi}{3} \frac{a^3}{M} (z_1^3 + z_2^3) = \frac{G}{3\pi} P^2 (z_1^3 + z_2^3) = \frac{G}{3\pi} P^2 z_1^3 (1 + \eta^3)$$

$$z_1 = \sqrt{\frac{\tau_1 \tau_2}{\eta}} \Rightarrow$$

$$\frac{1}{\rho} = \frac{G}{3\pi} P^2 (\tau_1 \tau_2)^{3/2} (\eta^{3/2} + \eta^{-3/2}) = \frac{\pi^2 G}{3} \frac{(t_1 t_2)^{3/2}}{P} (\eta^{-3/2} + \eta^{3/2})$$

And, if the two masses are known (or assumed) to be equal:

$$\frac{1}{\rho_1} = \frac{2\pi^2 G (t_1 t_2)^{3/2}}{3 P} \eta^{3/2} = \frac{2\pi^2 G (t_1 t_2)^{3/2}}{3 P} \left(\frac{F_1}{F_3 - F_2} \right)^{3/4}$$

Now, the hardest thing to measure (assuming no blending) will be t_2 (ingress time). This is relatively short, so few data points. Plus, one must actually understand limb darkening quite well to measure it. The only quantity susceptible to blending is η . If the system is blended by flux F_b , then all three fluxes F_1, F_3, F_3 are increased by this same amount. In this case,

$$\frac{d \ln \eta^2}{d F_b} = -\frac{1}{F_1} \Rightarrow \frac{d \ln \rho_1}{d F_b} = -\frac{3}{4} \frac{1}{F_1} \Rightarrow \Delta \ln \rho_1 = -\frac{3 F_b}{4 F_1}.$$

Blending can be controlled in two complementary ways. First, high-resolution images on 8 m class telescopes should be able to detect all sources within 2 FWHM of the target, down to 1–2% in *JHK*. Translating these fluxes into *I*-band will involve some error, but should be statistically unbiased.

Second, any ambient source within the optical PSF with 1–2% of target flux can be detected as follows. Since the periods are typically $P = 20$ days, the two sources will have relatively motion roughly 100 km/s, while the line-widths should be smaller by a factor $r/2a$, even if the stars are tidally locked. Therefore, the line systems of the two stars should be quite well separated, enabling excellent empirical templates of both from the ensemble of RV spectra. Then these templates can be subtracted from each spectrum, shifted by the fit velocity. The sum of the residuals of these fits will give a S/N \sim few spectrum of any ambient light, certainly enough to identify its source.

Table 1

OGLE-II field and lightcurve identification from Devor (2005), coordinates, $V - I$ colors, apparent magnitudes, relative radii and periods for the gold (first part) and silver (second part) sample of identified RG eclipsing binary pairs

| Field | ID | RA | DEC | $(V - I)$ | I | R_1/a | R_2/a | period [days] |
|-------|------|--|-------------|-----------|--------|---------|---------|---------------|
| 3 | 2325 | 17 ^h 53 ^m 15 ^s 31 | -30°07'57"2 | 2.398 | 16.977 | 0.375 | 0.263 | 4.488256 |
| 3 | 2823 | 17 ^h 53 ^m 55 ^s 27 | -30°05'18"9 | 2.133 | 17.214 | 0.329 | 0.249 | 3.930081 |
| 3 | 2929 | 17 ^h 53 ^m 45 ^s 96 | -30°04'33"6 | 2.245 | 17.604 | 0.370 | 0.276 | 3.471413 |
| 3 | 7715 | 17 ^h 53 ^m 31 ^s 11 | -29°34'38"7 | 2.417 | 16.969 | 0.345 | 0.222 | 5.883186 |
| 4 | 830 | 17 ^h 54 ^m 33 ^s 33 | -30°06'18"3 | 2.477 | 16.781 | 0.392 | 0.305 | 7.477364 |
| 4 | 831 | 17 ^h 54 ^m 35 ^s 36 | -30°06'23"2 | 2.326 | 17.744 | 0.392 | 0.346 | 2.403032 |
| 4 | 1290 | 17 ^h 55 ^m 01 ^s 80 | -30°03'44"6 | 2.388 | 17.356 | 0.346 | 0.268 | 4.055058 |
| 5 | 1889 | 17 ^h 50 ^m 35 ^s 23 | -30°09'19"5 | 3.664 | 18.061 | 0.362 | 0.279 | 7.024886 |
| 7 | 1089 | 18 ^h 08 ^m 53 ^s 56 | -31°54'48"1 | 1.362 | 16.659 | 0.310 | 0.280 | 3.112654 |
| 9 | 132 | 18 ^h 24 ^m 17 ^s 25 | -22°10'52"1 | 1.989 | 16.577 | 0.414 | 0.276 | 3.336563 |
| 9 | 1502 | 18 ^h 24 ^m 07 ^s 57 | -21°31'22"4 | 1.787 | 16.390 | 0.384 | 0.306 | 3.458615 |
| 13 | 1282 | 18 ^h 17 ^m 07 ^s 41 | -24°03'03"3 | 2.112 | 16.314 | 0.255 | 0.105 | 12.277672 |
| 14 | 3912 | 17 ^h 47 ^m 11 ^s 83 | -22°42'21"1 | 2.288 | 17.316 | 0.403 | 0.269 | 4.758608 |
| 24 | 1374 | 17 ^h 53 ^m 38 ^s 18 | -33°01'25"4 | 2.193 | 17.368 | 0.426 | 0.248 | 4.623804 |
| 24 | 2461 | 17 ^h 53 ^m 03 ^s 90 | -32°45'12"4 | 2.423 | 16.021 | 0.329 | 0.190 | 21.687112 |
| 30 | 1600 | 18 ^h 01 ^m 22 ^s 55 | -29°03'24"0 | 1.929 | 17.316 | 0.278 | 0.233 | 4.671058 |
| 30 | 6658 | 18 ^h 01 ^m 27 ^s 97 | -28°24'07"8 | 1.946 | 15.935 | 0.354 | 0.272 | 9.952315 |
| 31 | 631 | 18 ^h 02 ^m 14 ^s 25 | -28°56'11"2 | 1.945 | 16.331 | 0.370 | 0.289 | 3.937200 |
| 31 | 2641 | 18 ^h 02 ^m 10 ^s 51 | -28°30'10"2 | 1.768 | 16.657 | 0.307 | 0.222 | 5.033917 |
| 34 | 1369 | 17 ^h 58 ^m 11 ^s 35 | -29°24'54"4 | 2.610 | 17.027 | 0.410 | 0.251 | 6.113610 |
| 34 | 6500 | 17 ^h 57 ^m 57 ^s 95 | -28°48'09"3 | 2.045 | 17.238 | 0.360 | 0.261 | 3.436820 |
| 37 | 1846 | 17 ^h 52 ^m 30 ^s 15 | -30°11'44"6 | 2.331 | 17.367 | 0.344 | 0.311 | 2.934912 |
| 37 | 6396 | 17 ^h 52 ^m 35 ^s 36 | -29°40'28"6 | 2.619 | 16.767 | 0.294 | 0.190 | 7.772554 |
| 37 | 7093 | 17 ^h 52 ^m 15 ^s 51 | -29°36'14"2 | 3.147 | 17.517 | 0.254 | 0.232 | 6.784166 |
| 39 | 1159 | 17 ^h 55 ^m 53 ^s 47 | -30°02'53"9 | 2.385 | 17.154 | 0.369 | 0.217 | 4.455969 |
| 39 | 1604 | 17 ^h 55 ^m 31 ^s 28 | -29°59'03"9 | 2.574 | 18.199 | 0.411 | 0.320 | 2.430296 |
| 40 | 310 | 17 ^h 51 ^m 33 ^s 38 | -33°39'04"9 | 2.682 | 17.419 | 0.412 | 0.294 | 7.297005 |
| 40 | 621 | 17 ^h 51 ^m 18 ^s 82 | -33°33'59"8 | 2.459 | 17.004 | 0.436 | 0.204 | 7.069012 |
| 43 | 3095 | 17 ^h 35 ^m 17 ^s 21 | -26°47'27"8 | 2.439 | 16.954 | 0.359 | 0.279 | 4.740494 |
| 45 | 1064 | 18 ^h 04 ^m 04 ^s 03 | -30°03'52"2 | 2.048 | 14.894 | 0.199 | 0.058 | 78.765788 |
| 45 | 1155 | 18 ^h 03 ^m 44 ^s 62 | -30°01'55"3 | 1.956 | 17.143 | 0.319 | 0.243 | 5.400987 |
| 45 | 1522 | 18 ^h 03 ^m 42 ^s 13 | -29°53'05"3 | 1.640 | 17.350 | 0.364 | 0.358 | 2.424248 |
| 45 | 2170 | 18 ^h 03 ^m 57 ^s 10 | -29°39'36"7 | 2.122 | 15.881 | 0.247 | 0.090 | 23.699590 |
| 47 | 481 | 17 ^h 27 ^m 01 ^s 35 | -39°50'21"5 | 1.778 | 17.383 | 0.413 | 0.315 | 2.898527 |
| 1 | 1713 | 18 ^h 02 ^m 46 ^s 29 | -30°04'30"5 | 2.154 | 16.330 | 0.140 | 0.076 | 5.663370 |
| 1 | 2513 | 18 ^h 02 ^m 08 ^s 29 | -29°53'53"5 | 1.916 | 15.160 | 0.426 | 0.265 | 2.359235 |
| 1 | 2938 | 18 ^h 02 ^m 02 ^s 94 | -29°48'30"5 | 1.662 | 16.311 | 0.375 | 0.164 | 2.903954 |
| 1 | 3738 | 18 ^h 03 ^m 01 ^s 96 | -29°40'20"3 | 1.710 | 17.608 | 0.267 | 0.264 | 3.551679 |
| 1 | 3846 | 18 ^h 02 ^m 42 ^s 99 | -29°38'47"2 | 1.818 | 16.510 | 0.289 | 0.097 | 7.779557 |
| 1 | 3859 | 18 ^h 02 ^m 49 ^s 68 | -29°38'41"0 | 1.889 | 17.665 | 0.391 | 0.191 | 2.949637 |
| 2 | 892 | 18 ^h 04 ^m 35 ^s 40 | -29°11'58"1 | 1.764 | 16.882 | 0.416 | 0.145 | 4.541277 |
| 2 | 1301 | 18 ^h 04 ^m 24 ^s 76 | -29°07'16"1 | 1.628 | 16.505 | 0.253 | 0.079 | 6.464870 |
| 2 | 1800 | 18 ^h 04 ^m 09 ^s 41 | -29°00'56"9 | 1.506 | 17.095 | 0.300 | 0.199 | 2.339578 |
| 2 | 2542 | 18 ^h 04 ^m 54 ^s 38 | -28°53'55"9 | 1.395 | 15.973 | 0.360 | 0.208 | 3.085778 |

Table 1

Continued

| Field | ID | RA | DEC | (V - I) | I | R ₁ /a | R ₂ /a | period [days] |
|-------|------|--|--------------|---------|--------|-------------------|-------------------|---------------|
| 2 | 3673 | 18 ^h 04 ^m 45 ^s 22 | -28°42'13''0 | 1.673 | 17.379 | 0.322 | 0.088 | 12.985678 |
| 2 | 3894 | 18 ^h 04 ^m 19 ^s 55 | -28°39'46''3 | 1.597 | 17.256 | 0.338 | 0.164 | 3.335057 |
| 2 | 4754 | 18 ^h 04 ^m 10 ^s 21 | -28°30'05''0 | 1.662 | 17.289 | 0.325 | 0.203 | 2.130568 |
| 3 | 1149 | 17 ^h 53 ^m 11 ^s 82 | -30°16'45''6 | 2.844 | 16.814 | 0.421 | 0.187 | 3.295681 |
| 3 | 1688 | 17 ^h 53 ^m 58 ^s 88 | -30°13'45''6 | 2.052 | 17.444 | 0.381 | 0.214 | 2.479170 |
| 3 | 2195 | 17 ^h 53 ^m 15 ^s 24 | -30°08'44''6 | 2.224 | 16.433 | 0.418 | 0.159 | 3.179790 |
| 3 | 3488 | 17 ^h 53 ^m 53 ^s 48 | -30°01'21''8 | 2.328 | 18.132 | 0.259 | 0.204 | 2.156910 |
| 3 | 3489 | 17 ^h 53 ^m 54 ^s 82 | -30°00'46''7 | 2.652 | 16.082 | 0.283 | 0.082 | 2.943854 |
| 3 | 3547 | 17 ^h 53 ^m 25 ^s 67 | -30°00'01''5 | 2.635 | 17.816 | 0.266 | 0.228 | 2.474109 |
| 3 | 3744 | 17 ^h 54 ^m 04 ^s 47 | -29°59'15''8 | 2.335 | 17.619 | 0.335 | 0.272 | 3.511041 |
| 3 | 6413 | 17 ^h 53 ^m 31 ^s 09 | -29°41'39''3 | 2.382 | 16.943 | 0.322 | 0.182 | 8.528036 |
| 3 | 8222 | 17 ^h 53 ^m 55 ^s 24 | -29°31'35''3 | 2.469 | 17.493 | 0.297 | 0.242 | 7.623718 |
| 3 | 8395 | 17 ^h 53 ^m 16 ^s 26 | -29°30'30''0 | 3.095 | 17.369 | 0.418 | 0.257 | 5.337132 |
| 4 | 1047 | 17 ^h 54 ^m 10 ^s 50 | -30°04'31''6 | 2.063 | 16.928 | 0.316 | 0.176 | 2.075691 |
| 4 | 1120 | 17 ^h 54 ^m 44 ^s 27 | -30°04'11''8 | 2.206 | 16.953 | 0.448 | 0.227 | 7.343176 |
| 4 | 1224 | 17 ^h 54 ^m 21 ^s 76 | -30°03'07''7 | 2.226 | 17.284 | 0.362 | 0.216 | 5.331105 |
| 4 | 1289 | 17 ^h 54 ^m 57 ^s 96 | -30°03'31''4 | 2.317 | 18.168 | 0.267 | 0.200 | 3.543221 |
| 4 | 3707 | 17 ^h 54 ^m 58 ^s 48 | -29°49'18''1 | 1.824 | 17.100 | 0.300 | 0.198 | 2.381842 |
| 4 | 4049 | 17 ^h 54 ^m 41 ^s 33 | -29°47'16''7 | 2.424 | 16.459 | 0.119 | 0.103 | 3.842130 |
| 4 | 4449 | 17 ^h 54 ^m 07 ^s 59 | -29°44'58''6 | 2.321 | 15.552 | 0.572 | 0.129 | 2.269646 |
| 4 | 4564 | 17 ^h 54 ^m 57 ^s 61 | -29°45'02''3 | 2.502 | 17.463 | 0.328 | 0.211 | 3.350001 |
| 4 | 5392 | 17 ^h 54 ^m 17 ^s 17 | -29°39'20''2 | 2.294 | 16.289 | 0.162 | 0.105 | 2.820490 |
| 4 | 6839 | 17 ^h 54 ^m 39 ^s 93 | -29°30'30''7 | 2.033 | 17.402 | 0.319 | 0.227 | 2.379704 |
| 4 | 6905 | 17 ^h 54 ^m 18 ^s 89 | -29°29'39''7 | 2.137 | 18.454 | 0.305 | 0.296 | 3.514754 |
| 4 | 7346 | 17 ^h 54 ^m 12 ^s 23 | -29°27'05''6 | 2.371 | 17.937 | 0.323 | 0.247 | 2.697201 |
| 4 | 8604 | 17 ^h 54 ^m 10 ^s 56 | -29°18'18''2 | 2.488 | 18.280 | 0.201 | 0.128 | 4.274822 |
| 5 | 5124 | 17 ^h 49 ^m 58 ^s 22 | -29°44'04''5 | 4.193 | 17.418 | 0.169 | 0.125 | 5.659006 |
| 6 | 358 | 18 ^h 07 ^m 46 ^s 98 | -32°29'20''1 | 1.739 | 15.439 | 0.246 | 0.064 | 3.476010 |
| 6 | 598 | 18 ^h 08 ^m 28 ^s 11 | -32°24'58''7 | 1.731 | 18.033 | 0.326 | 0.158 | 2.457010 |
| 6 | 1214 | 18 ^h 08 ^m 34 ^s 60 | -32°12'28''4 | 1.683 | 16.958 | 0.431 | 0.242 | 5.688314 |
| 6 | 1517 | 18 ^h 07 ^m 56 ^s 87 | -32°06'12''5 | 1.335 | 17.511 | 0.102 | 0.078 | 6.417924 |
| 7 | 299 | 18 ^h 08 ^m 51 ^s 59 | -32°23'13''2 | 1.504 | 18.265 | 0.087 | 0.078 | 4.048338 |
| 7 | 605 | 18 ^h 09 ^m 14 ^s 45 | -32°10'42''7 | 1.865 | 17.022 | 0.383 | 0.324 | 4.259042 |
| 7 | 1494 | 18 ^h 08 ^m 52 ^s 25 | -31°42'44''0 | 1.410 | 17.626 | 0.134 | 0.113 | 3.341994 |
| 8 | 430 | 18 ^h 23 ^m 30 ^s 17 | -22°03'23''6 | 2.026 | 16.850 | 0.416 | 0.076 | 3.499018 |
| 8 | 829 | 18 ^h 23 ^m 23 ^s 13 | -21°54'38''5 | 1.969 | 17.260 | 0.239 | 0.198 | 4.084482 |
| 10 | 1924 | 18 ^h 20 ^m 06 ^s 01 | -22°09'22''3 | 1.951 | 17.836 | 0.215 | 0.111 | 4.128718 |
| 10 | 2053 | 18 ^h 20 ^m 00 ^s 77 | -22°07'06''5 | 1.778 | 16.923 | 0.311 | 0.286 | 3.729120 |
| 11 | 1231 | 18 ^h 20 ^m 54 ^s 55 | -22°21'07''1 | 1.910 | 16.945 | 0.349 | 0.245 | 3.733986 |
| 11 | 1934 | 18 ^h 21 ^m 22 ^s 82 | -22°03'02''7 | 2.119 | 16.015 | 0.289 | 0.106 | 11.554690 |
| 12 | 1664 | 18 ^h 16 ^m 26 ^s 54 | -24°00'08''6 | 2.071 | 17.492 | 0.180 | 0.121 | 2.812648 |
| 12 | 2249 | 18 ^h 16 ^m 22 ^s 47 | -23°50'50''8 | 1.909 | 17.937 | 0.177 | 0.109 | 4.133296 |
| 12 | 3118 | 18 ^h 15 ^m 57 ^s 17 | -23°35'39''6 | 2.105 | 17.756 | 0.215 | 0.111 | 2.731754 |
| 13 | 515 | 18 ^h 16 ^m 54 ^s 03 | -24°16'52''7 | 2.179 | 17.315 | 0.209 | 0.198 | 2.280115 |
| 13 | 643 | 18 ^h 17 ^m 21 ^s 43 | -24°15'08''1 | 2.228 | 18.266 | 0.429 | 0.229 | 2.543559 |
| 13 | 748 | 18 ^h 16 ^m 47 ^s 11 | -24°11'53''1 | 2.477 | 17.513 | 0.184 | 0.085 | 3.086584 |
| 14 | 748 | 17 ^h 46 ^m 47 ^s 93 | -23°24'30''5 | 2.054 | 16.809 | 0.270 | 0.116 | 3.205315 |

Table 1

Continued

| Field | ID | RA | DEC | (V - I) | I | R ₁ /a | R ₂ /a | period [days] |
|-------|------|---|--------------|---------|--------|-------------------|-------------------|---------------|
| 14 | 842 | 17 ^h 46 ^m 34 ^s .66 | -23°22'50".8 | 2.108 | 15.063 | 0.281 | 0.123 | 4.724715 |
| 14 | 1246 | 17 ^h 47 ^m 16 ^s .93 | -23°16'39".8 | 2.224 | 16.485 | 0.256 | 0.092 | 10.525937 |
| 14 | 1360 | 17 ^h 46 ^m 51 ^s .72 | -23°14'51".2 | 2.042 | 18.241 | 0.278 | 0.107 | 5.335997 |
| 14 | 2296 | 17 ^h 47 ^m 19 ^s .49 | -23°03'42".5 | 2.428 | 15.460 | 0.240 | 0.056 | 2.429135 |
| 14 | 3223 | 17 ^h 47 ^m 01 ^s .51 | -22°53'10".2 | 2.043 | 17.372 | 0.307 | 0.168 | 2.697653 |
| 14 | 3755 | 17 ^h 46 ^m 38 ^s .18 | -22°43'40".9 | 1.996 | 17.495 | 0.317 | 0.237 | 2.063695 |
| 15 | 529 | 17 ^h 47 ^m 50 ^s .68 | -23°25'54".5 | 2.122 | 17.324 | 0.371 | 0.172 | 4.172854 |
| 15 | 631 | 17 ^h 48 ^m 16 ^s .06 | -23°25'22".9 | 2.125 | 17.695 | 0.285 | 0.228 | 2.886554 |
| 15 | 851 | 17 ^h 48 ^m 12 ^s .09 | -23°21'51".4 | 2.277 | 17.754 | 0.385 | 0.191 | 3.268354 |
| 15 | 1341 | 17 ^h 47 ^m 50 ^s .79 | -23°15'13".1 | 2.424 | 17.552 | 0.198 | 0.116 | 2.767438 |
| 15 | 2256 | 17 ^h 48 ^m 13 ^s .84 | -23°02'45".3 | 2.297 | 17.944 | 0.376 | 0.270 | 2.562922 |
| 16 | 147 | 18 ^h 10 ^m 03 ^s .80 | -26°44'29".4 | 2.035 | 18.238 | 0.190 | 0.094 | 7.611000 |
| 16 | 443 | 18 ^h 09 ^m 55 ^s .54 | -26°40'37".0 | 2.073 | 17.613 | 0.338 | 0.229 | 2.515553 |
| 16 | 722 | 18 ^h 09 ^m 58 ^s .67 | -26°36'52".8 | 2.165 | 17.419 | 0.406 | 0.268 | 5.064416 |
| 16 | 2304 | 18 ^h 09 ^m 58 ^s .50 | -26°19'18".5 | 1.821 | 16.691 | 0.356 | 0.137 | 3.572162 |
| 16 | 3066 | 18 ^h 09 ^m 45 ^s .75 | -26°10'33".8 | 1.977 | 17.956 | 0.287 | 0.179 | 4.327591 |
| 17 | 417 | 18 ^h 11 ^m 10 ^s .05 | -26°34'35".0 | 1.639 | 16.783 | 0.369 | 0.235 | 2.958341 |
| 17 | 1576 | 18 ^h 10 ^m 51 ^s .97 | -26°21'58".3 | 1.902 | 17.489 | 0.418 | 0.125 | 3.480961 |
| 17 | 1577 | 18 ^h 10 ^m 58 ^s .42 | -26°22'06".7 | 2.019 | 16.847 | 0.181 | 0.130 | 20.532350 |
| 17 | 2366 | 18 ^h 11 ^m 07 ^s .56 | -26°11'28".4 | 1.663 | 17.709 | 0.150 | 0.136 | 2.771794 |
| 17 | 4107 | 18 ^h 11 ^m 07 ^s .22 | -25°49'57".8 | 1.863 | 16.939 | 0.367 | 0.153 | 3.584156 |
| 18 | 667 | 18 ^h 06 ^m 37 ^s .36 | -27°33'42".9 | 2.116 | 16.079 | 0.172 | 0.074 | 9.504011 |
| 18 | 1201 | 18 ^h 06 ^m 42 ^s .52 | -27°28'03".3 | 1.553 | 17.341 | 0.274 | 0.207 | 3.936500 |
| 18 | 2492 | 18 ^h 06 ^m 38 ^s .20 | -27°17'03".5 | 1.509 | 17.265 | 0.254 | 0.101 | 3.187028 |
| 18 | 3232 | 18 ^h 07 ^m 07 ^s .99 | -27°09'23".8 | 1.668 | 16.559 | 0.207 | 0.117 | 2.345478 |
| 18 | 3834 | 18 ^h 06 ^m 33 ^s .83 | -27°03'35".0 | 1.649 | 17.338 | 0.153 | 0.082 | 4.064586 |
| 18 | 3942 | 18 ^h 06 ^m 43 ^s .70 | -27°02'38".1 | 1.595 | 16.204 | 0.259 | 0.242 | 4.271732 |
| 18 | 4093 | 18 ^h 07 ^m 25 ^s .56 | -27°01'43".0 | 1.854 | 17.096 | 0.332 | 0.229 | 3.373929 |
| 18 | 4246 | 18 ^h 06 ^m 59 ^s .39 | -27°00'14".5 | 1.552 | 17.062 | 0.380 | 0.267 | 5.194025 |
| 18 | 4368 | 18 ^h 07 ^m 03 ^s .12 | -26°59'28".2 | 1.596 | 17.437 | 0.213 | 0.141 | 2.582868 |
| 19 | 3463 | 18 ^h 07 ^m 44 ^s .88 | -27°02'14".3 | 2.022 | 17.794 | 0.310 | 0.207 | 2.165127 |
| 19 | 4115 | 18 ^h 08 ^m 31 ^s .28 | -26°56'27".2 | 1.699 | 17.174 | 0.325 | 0.244 | 2.022135 |
| 20 | 508 | 17 ^h 59 ^m 17 ^s .21 | -29°15'46".0 | 1.784 | 16.925 | 0.346 | 0.246 | 6.437626 |
| 20 | 625 | 17 ^h 59 ^m 11 ^s .17 | -29°14'26".7 | 1.713 | 16.759 | 0.267 | 0.160 | 2.156676 |
| 20 | 726 | 17 ^h 59 ^m 12 ^s .62 | -29°13'58".6 | 1.620 | 17.047 | 0.359 | 0.323 | 3.220336 |
| 20 | 764 | 17 ^h 59 ^m 37 ^s .56 | -29°13'20".1 | 1.788 | 17.347 | 0.308 | 0.134 | 4.828995 |
| 20 | 1218 | 17 ^h 59 ^m 32 ^s .08 | -29°09'34".2 | 1.773 | 17.572 | 0.303 | 0.250 | 4.204415 |
| 20 | 3228 | 17 ^h 59 ^m 39 ^s .47 | -28°49'45".6 | 2.033 | 15.511 | 0.301 | 0.084 | 2.761122 |
| 20 | 3507 | 17 ^h 59 ^m 23 ^s .84 | -28°47'26".0 | 1.637 | 17.043 | 0.358 | 0.250 | 2.431410 |
| 20 | 3703 | 17 ^h 59 ^m 09 ^s .40 | -28°45'47".1 | 2.053 | 18.174 | 0.200 | 0.182 | 7.134314 |
| 20 | 3831 | 17 ^h 59 ^m 26 ^s .04 | -28°44'13".9 | 1.958 | 16.494 | 0.121 | 0.071 | 3.034756 |
| 20 | 4260 | 17 ^h 59 ^m 36 ^s .54 | -28°40'51".1 | 1.833 | 17.474 | 0.214 | 0.107 | 4.127868 |
| 20 | 5428 | 17 ^h 58 ^m 56 ^s .59 | -28°29'28".5 | 2.034 | 17.265 | 0.269 | 0.198 | 2.185926 |
| 21 | 564 | 18 ^h 00 ^m 46 ^s .24 | -29°15'53".4 | 1.970 | 17.238 | 0.365 | 0.255 | 2.753914 |
| 21 | 1563 | 18 ^h 00 ^m 34 ^s .98 | -29°07'43".6 | 1.954 | 15.966 | 0.184 | 0.032 | 28.799444 |
| 21 | 1588 | 18 ^h 00 ^m 43 ^s .62 | -29°08'08".8 | 1.733 | 15.282 | 0.312 | 0.224 | 3.740300 |
| 21 | 2360 | 18 ^h 00 ^m 22 ^s .92 | -29°01'28".2 | 1.543 | 16.283 | 0.520 | 0.176 | 3.589142 |
| 21 | 2601 | 18 ^h 00 ^m 06 ^s .28 | -29°00'11".0 | 1.579 | 17.763 | 0.230 | 0.132 | 3.180098 |

Table 1

Continued

| Field | ID | RA | DEC | (V - I) | I | R ₁ /a | R ₂ /a | period [days] |
|-------|------|---|--------------|---------|--------|-------------------|-------------------|---------------|
| 21 | 2750 | 18 ^h 00 ^m 35 ^s .67 | -28°58'56".2 | 1.534 | 17.480 | 0.325 | 0.255 | 2.220600 |
| 21 | 3596 | 18 ^h 00 ^m 09 ^s .93 | -28°52'40".9 | 2.038 | 18.247 | 0.360 | 0.334 | 4.252551 |
| 21 | 4732 | 18 ^h 00 ^m 33 ^s .33 | -28°45'29".7 | 2.181 | 17.291 | 0.223 | 0.062 | 2.871256 |
| 21 | 6233 | 18 ^h 00 ^m 03 ^s .29 | -28°33'32".7 | 2.488 | 16.801 | 0.415 | 0.141 | 2.923352 |
| 21 | 6795 | 18 ^h 00 ^m 09 ^s .54 | -28°29'11".3 | 1.806 | 16.978 | 0.351 | 0.203 | 5.214180 |
| 21 | 7051 | 18 ^h 00 ^m 42 ^s .73 | -28°27'10".0 | 1.867 | 17.868 | 0.323 | 0.204 | 2.701986 |
| 21 | 7356 | 18 ^h 00 ^m 25 ^s .77 | -28°24'37".8 | 1.944 | 16.954 | 0.316 | 0.307 | 4.641814 |
| 22 | 10 | 17 ^h 56 ^m 27 ^s .07 | -31°15'31".6 | 1.988 | 17.542 | 0.285 | 0.196 | 4.378102 |
| 22 | 114 | 17 ^h 57 ^m 20 ^s .34 | -31°14'52".1 | 2.215 | 17.198 | 0.392 | 0.203 | 4.809705 |
| 22 | 222 | 17 ^h 56 ^m 23 ^s .41 | -31°13'10".8 | 2.259 | 17.795 | 0.155 | 0.057 | 11.372206 |
| 22 | 1335 | 17 ^h 57 ^m 12 ^s .80 | -31°01'58".1 | 1.774 | 17.769 | 0.405 | 0.211 | 2.119743 |
| 22 | 2938 | 17 ^h 56 ^m 28 ^s .02 | -30°47'05".7 | 1.761 | 16.769 | 0.240 | 0.113 | 4.996538 |
| 23 | 293 | 17 ^h 57 ^m 23 ^s .92 | -31°36'32".2 | 2.103 | 18.642 | 0.208 | 0.083 | 5.482078 |
| 23 | 1425 | 17 ^h 57 ^m 34 ^s .18 | -31°23'01".8 | 2.346 | 17.864 | 0.274 | 0.241 | 2.203385 |
| 23 | 1695 | 17 ^h 57 ^m 38 ^s .45 | -31°19'27".1 | 2.601 | 17.894 | 0.276 | 0.219 | 2.837150 |
| 23 | 3566 | 17 ^h 57 ^m 44 ^s .81 | -30°58'12".4 | 2.299 | 18.165 | 0.446 | 0.227 | 2.023772 |
| 23 | 3832 | 17 ^h 57 ^m 38 ^s .48 | -30°55'07".3 | 2.678 | 15.592 | 0.481 | 0.085 | 36.548702 |
| 24 | 1797 | 17 ^h 53 ^m 38 ^s .44 | -32°55'12".2 | 2.144 | 17.542 | 0.350 | 0.227 | 8.378970 |
| 24 | 2166 | 17 ^h 53 ^m 03 ^s .75 | -32°49'24".8 | 2.029 | 16.710 | 0.304 | 0.147 | 6.788291 |
| 24 | 2463 | 17 ^h 53 ^m 04 ^s .50 | -32°45'05".9 | 2.564 | 15.956 | 0.266 | 0.075 | 2.846186 |
| 25 | 425 | 17 ^h 54 ^m 39 ^s .82 | -33°11'54".2 | 2.022 | 17.896 | 0.357 | 0.308 | 2.807364 |
| 25 | 2256 | 17 ^h 54 ^m 16 ^s .80 | -32°37'23".3 | 1.886 | 17.655 | 0.446 | 0.233 | 3.888740 |
| 25 | 2800 | 17 ^h 54 ^m 22 ^s .11 | -32°28'52".9 | 1.867 | 17.709 | 0.234 | 0.117 | 4.863817 |
| 25 | 2836 | 17 ^h 53 ^m 59 ^s .11 | -32°28'01".3 | 1.870 | 17.235 | 0.357 | 0.255 | 2.113844 |
| 26 | 572 | 17 ^h 46 ^m 59 ^s .47 | -35°19'42".8 | 2.003 | 16.379 | 0.215 | 0.084 | 13.478680 |
| 26 | 946 | 17 ^h 46 ^m 58 ^s .93 | -35°15'02".0 | 1.814 | 17.455 | 0.287 | 0.190 | 2.131286 |
| 26 | 1376 | 17 ^h 47 ^m 03 ^s .47 | -35°09'54".2 | 1.838 | 17.619 | 0.348 | 0.312 | 2.009605 |
| 26 | 3703 | 17 ^h 47 ^m 10 ^s .75 | -34°43'40".4 | 1.682 | 15.740 | 0.116 | 0.029 | 2.620312 |
| 26 | 3875 | 17 ^h 47 ^m 08 ^s .15 | -34°43'16".5 | 1.732 | 17.322 | 0.117 | 0.076 | 2.396786 |
| 26 | 4375 | 17 ^h 47 ^m 45 ^s .91 | -34°36'39".6 | 2.014 | 18.062 | 0.197 | 0.122 | 2.961308 |
| 26 | 4395 | 17 ^h 46 ^m 46 ^s .31 | -34°36'26".1 | 2.021 | 17.902 | 0.171 | 0.125 | 3.688354 |
| 27 | 323 | 17 ^h 48 ^m 23 ^s .02 | -35°32'00".8 | 1.524 | 16.950 | 0.120 | 0.051 | 2.038052 |
| 27 | 646 | 17 ^h 48 ^m 20 ^s .08 | -35°26'48".3 | 1.599 | 17.457 | 0.357 | 0.325 | 3.404542 |
| 27 | 1512 | 17 ^h 48 ^m 30 ^s .63 | -35°15'20".6 | 1.594 | 16.877 | 0.312 | 0.284 | 3.744963 |
| 27 | 1587 | 17 ^h 47 ^m 58 ^s .47 | -35°13'20".4 | 1.638 | 17.604 | 0.290 | 0.132 | 2.221579 |
| 27 | 2801 | 17 ^h 47 ^m 57 ^s .32 | -34°55'17".3 | 1.639 | 17.837 | 0.257 | 0.127 | 4.287232 |
| 28 | 974 | 17 ^h 46 ^m 33 ^s .81 | -36°56'26".9 | 1.694 | 17.141 | 0.181 | 0.059 | 3.625968 |
| 28 | 1355 | 17 ^h 46 ^m 59 ^s .43 | -36°43'51".2 | 1.735 | 18.333 | 0.271 | 0.222 | 2.050652 |
| 29 | 491 | 17 ^h 47 ^m 48 ^s .95 | -37°21'59".4 | 1.596 | 16.120 | 0.386 | 0.212 | 3.137304 |
| 29 | 943 | 17 ^h 47 ^m 53 ^s .46 | -37°11'14".8 | 1.603 | 17.413 | 0.226 | 0.125 | 6.781612 |
| 29 | 1001 | 17 ^h 48 ^m 13 ^s .64 | -37°10'05".6 | 1.461 | 16.225 | 0.303 | 0.238 | 3.450851 |
| 29 | 1063 | 17 ^h 47 ^m 57 ^s .24 | -37°08'22".1 | 1.574 | 16.961 | 0.398 | 0.165 | 2.255049 |
| 29 | 1149 | 17 ^h 48 ^m 43 ^s .11 | -37°06'33".9 | 1.812 | 17.158 | 0.220 | 0.207 | 8.651742 |
| 29 | 1755 | 17 ^h 48 ^m 12 ^s .65 | -36°52'44".1 | 1.949 | 16.930 | 0.463 | 0.208 | 10.219748 |
| 30 | 983 | 18 ^h 01 ^m 12 ^s .34 | -29°08'57".4 | 1.968 | 16.868 | 0.101 | 0.075 | 36.279276 |
| 30 | 1034 | 18 ^h 01 ^m 51 ^s .72 | -29°08'47".0 | 1.971 | 17.219 | 0.304 | 0.153 | 3.515654 |
| 30 | 1558 | 18 ^h 00 ^m 57 ^s .01 | -29°03'37".4 | 1.763 | 16.068 | 0.139 | 0.043 | 5.385688 |

Table 1

Continued

| Field | ID | RA | DEC | (V-I) | I | R ₁ /a | R ₂ /a | period [days] |
|-------|------|---|--------------|-------|--------|-------------------|-------------------|---------------|
| 30 | 2126 | 18 ^h 01 ^m 53 ^s .58 | -28°59'19".6 | 1.889 | 17.735 | 0.396 | 0.313 | 2.539593 |
| 30 | 2158 | 18 ^h 01 ^m 07 ^s .93 | -28°58'25".6 | 1.642 | 16.387 | 0.390 | 0.293 | 2.205462 |
| 30 | 2508 | 18 ^h 01 ^m 24 ^s .79 | -28°55'21".9 | 1.791 | 17.463 | 0.311 | 0.157 | 5.518564 |
| 30 | 3167 | 18 ^h 01 ^m 48 ^s .86 | -28°51'10".8 | 1.615 | 17.629 | 0.160 | 0.111 | 3.254480 |
| 30 | 5566 | 18 ^h 01 ^m 11 ^s .19 | -28°32'38".6 | 1.661 | 17.393 | 0.193 | 0.134 | 4.206418 |
| 30 | 5978 | 18 ^h 00 ^m 57 ^s .98 | -28°29'09".2 | 1.774 | 16.501 | 0.173 | 0.067 | 10.134768 |
| 31 | 399 | 18 ^h 01 ^m 53 ^s .58 | -28°59'19".7 | 1.831 | 17.735 | 0.389 | 0.314 | 2.539666 |
| 31 | 2277 | 18 ^h 02 ^m 26 ^s .01 | -28°34'28".9 | 2.109 | 17.576 | 0.311 | 0.179 | 3.181014 |
| 31 | 2670 | 18 ^h 02 ^m 30 ^s .81 | -28°29'58".1 | 1.951 | 17.559 | 0.412 | 0.260 | 2.312017 |
| 31 | 2793 | 18 ^h 01 ^m 53 ^s .97 | -28°27'47".4 | 1.789 | 17.137 | 0.201 | 0.105 | 6.405328 |
| 31 | 3308 | 18 ^h 02 ^m 27 ^s .26 | -28°23'22".3 | 1.777 | 17.224 | 0.365 | 0.180 | 2.686944 |
| 31 | 4092 | 18 ^h 02 ^m 49 ^s .03 | -28°16'33".3 | 1.659 | 17.698 | 0.295 | 0.231 | 3.067622 |
| 31 | 4328 | 18 ^h 02 ^m 25 ^s .28 | -28°13'40".1 | 1.593 | 17.387 | 0.104 | 0.070 | 7.872418 |
| 31 | 4787 | 18 ^h 02 ^m 49 ^s .76 | -28°09'59".3 | 1.556 | 17.561 | 0.420 | 0.304 | 3.079226 |
| 32 | 926 | 18 ^h 03 ^m 26 ^s .66 | -28°54'40".6 | 1.544 | 17.382 | 0.107 | 0.053 | 13.887762 |
| 32 | 1504 | 18 ^h 03 ^m 37 ^s .95 | -28°48'24".6 | 1.680 | 17.251 | 0.273 | 0.167 | 6.526399 |
| 32 | 1928 | 18 ^h 03 ^m 54 ^s .07 | -28°43'54".9 | 1.738 | 16.620 | 0.383 | 0.251 | 4.992396 |
| 32 | 2053 | 18 ^h 03 ^m 34 ^s .10 | -28°41'56".9 | 1.686 | 17.126 | 0.172 | 0.111 | 7.414870 |
| 32 | 3061 | 18 ^h 03 ^m 17 ^s .72 | -28°31'15".5 | 2.076 | 17.038 | 0.266 | 0.110 | 5.346271 |
| 32 | 3753 | 18 ^h 03 ^m 19 ^s .86 | -28°23'36".5 | 1.752 | 17.151 | 0.184 | 0.054 | 9.886980 |
| 32 | 4589 | 18 ^h 03 ^m 56 ^s .25 | -28°14'43".9 | 1.569 | 16.890 | 0.153 | 0.087 | 5.627108 |
| 33 | 547 | 18 ^h 05 ^m 36 ^s .60 | -29°13'14".3 | 1.840 | 17.417 | 0.383 | 0.170 | 3.463207 |
| 33 | 686 | 18 ^h 05 ^m 26 ^s .29 | -29°11'57".4 | 1.612 | 17.791 | 0.162 | 0.097 | 4.095290 |
| 33 | 1629 | 18 ^h 05 ^m 21 ^s .08 | -28°59'58".8 | 1.760 | 17.658 | 0.305 | 0.162 | 2.058984 |
| 33 | 2278 | 18 ^h 05 ^m 26 ^s .10 | -28°52'17".1 | 1.663 | 18.171 | 0.396 | 0.165 | 2.013036 |
| 33 | 3188 | 18 ^h 05 ^m 45 ^s .64 | -28°42'47".6 | 1.867 | 17.858 | 0.265 | 0.191 | 6.148376 |
| 34 | 420 | 17 ^h 58 ^m 18 ^s .98 | -29°32'57".1 | 2.097 | 17.302 | 0.277 | 0.139 | 2.231450 |
| 34 | 793 | 17 ^h 57 ^m 50 ^s .07 | -29°29'10".9 | 1.857 | 17.068 | 0.310 | 0.200 | 7.976383 |
| 34 | 1615 | 17 ^h 58 ^m 36 ^s .95 | -29°22'51".7 | 2.005 | 17.930 | 0.376 | 0.265 | 2.540265 |
| 34 | 1706 | 17 ^h 58 ^m 20 ^s .31 | -29°22'39".9 | 1.919 | 17.476 | 0.283 | 0.079 | 4.267768 |
| 34 | 1951 | 17 ^h 58 ^m 35 ^s .51 | -29°20'59".3 | 1.838 | 17.803 | 0.313 | 0.295 | 2.224765 |
| 34 | 2456 | 17 ^h 58 ^m 05 ^s .20 | -29°16'05".0 | 2.114 | 17.097 | 0.248 | 0.080 | 8.471958 |
| 34 | 2580 | 17 ^h 58 ^m 20 ^s .21 | -29°14'57".9 | 1.779 | 17.759 | 0.127 | 0.093 | 6.439528 |
| 34 | 2823 | 17 ^h 58 ^m 33 ^s .05 | -29°13'31".2 | 1.583 | 16.233 | 0.160 | 0.045 | 3.521810 |
| 34 | 2973 | 17 ^h 58 ^m 42 ^s .81 | -29°12'15".3 | 1.649 | 16.020 | 0.369 | 0.202 | 3.183053 |
| 34 | 5744 | 17 ^h 58 ^m 04 ^s .66 | -28°53'04".9 | 2.026 | 17.878 | 0.158 | 0.089 | 5.301156 |
| 35 | 2440 | 18 ^h 04 ^m 06 ^s .62 | -27°58'54".6 | 1.793 | 17.764 | 0.312 | 0.198 | 2.022147 |
| 35 | 2508 | 18 ^h 04 ^m 02 ^s .60 | -27°58'23".6 | 1.722 | 14.118 | 0.210 | 0.031 | 21.505206 |
| 35 | 2897 | 18 ^h 04 ^m 36 ^s .18 | -27°54'27".0 | 2.493 | 16.517 | 0.335 | 0.222 | 2.453367 |
| 35 | 4121 | 18 ^h 04 ^m 27 ^s .93 | -27°41'05".1 | 1.864 | 16.660 | 0.437 | 0.248 | 2.551206 |
| 35 | 4556 | 18 ^h 04 ^m 38 ^s .36 | -27°36'26".2 | 1.624 | 17.057 | 0.200 | 0.092 | 4.054498 |
| 35 | 4721 | 18 ^h 04 ^m 11 ^s .40 | -27°33'39".3 | 1.841 | 15.595 | 0.317 | 0.121 | 2.759243 |
| 36 | 1929 | 18 ^h 05 ^m 47 ^s .36 | -28°13'03".3 | 1.910 | 16.848 | 0.393 | 0.173 | 8.543916 |
| 36 | 3762 | 18 ^h 05 ^m 05 ^s .62 | -28°00'35".3 | 1.639 | 16.801 | 0.128 | 0.050 | 2.586147 |
| 36 | 4333 | 18 ^h 05 ^m 31 ^s .34 | -27°57'11".9 | 1.964 | 17.726 | 0.389 | 0.138 | 3.928802 |
| 36 | 4493 | 18 ^h 05 ^m 51 ^s .25 | -27°56'20".9 | 1.701 | 17.319 | 0.292 | 0.249 | 3.118629 |
| 36 | 4494 | 18 ^h 05 ^m 55 ^s .08 | -27°56'12".2 | 1.992 | 17.223 | 0.330 | 0.271 | 2.910082 |

Table 1

Concluded

| Field | ID | RA | DEC | (V - I) | I | R ₁ /a | R ₂ /a | period [days] |
|-------|------|---|--------------|---------|--------|-------------------|-------------------|---------------|
| 36 | 7720 | 18 ^h 05 ^m 37 ^s .14 | -27°36'22".0 | 1.613 | 17.819 | 0.239 | 0.161 | 3.115270 |
| 37 | 956 | 17 ^h 52 ^m 52 ^s .82 | -30°18'52".1 | 2.442 | 17.944 | 0.334 | 0.254 | 3.262918 |
| 37 | 2068 | 17 ^h 52 ^m 22 ^s .28 | -30°09'18".0 | 2.722 | 18.234 | 0.388 | 0.296 | 3.662674 |
| 37 | 2768 | 17 ^h 52 ^m 19 ^s .88 | -30°05'22".0 | 2.730 | 17.333 | 0.391 | 0.318 | 5.733310 |
| 37 | 3186 | 17 ^h 52 ^m 35 ^s .96 | -30°02'52".3 | 3.339 | 17.570 | 0.310 | 0.211 | 5.098516 |
| 37 | 3240 | 17 ^h 52 ^m 05 ^s .16 | -30°01'32".7 | 3.122 | 18.193 | 0.250 | 0.199 | 3.091703 |
| 37 | 4541 | 17 ^h 52 ^m 06 ^s .26 | -29°53'15".8 | 2.800 | 16.147 | 0.435 | 0.076 | 2.907292 |
| 37 | 6333 | 17 ^h 52 ^m 13 ^s .81 | -29°40'19".7 | 2.973 | 18.570 | 0.290 | 0.267 | 2.943085 |
| 37 | 6549 | 17 ^h 52 ^m 52 ^s .89 | -29°39'27".2 | 2.724 | 17.381 | 0.275 | 0.164 | 2.647908 |
| 37 | 7240 | 17 ^h 52 ^m 02 ^s .98 | -29°35'30".7 | 3.491 | 17.082 | 0.300 | 0.087 | 2.012917 |
| 37 | 8237 | 17 ^h 52 ^m 51 ^s .31 | -29°30'29".8 | 2.834 | 17.937 | 0.426 | 0.259 | 3.955137 |
| 38 | 1003 | 18 ^h 01 ^m 29 ^s .06 | -30°14'16".6 | 1.901 | 17.678 | 0.321 | 0.236 | 2.495866 |
| 38 | 1675 | 18 ^h 01 ^m 37 ^s .77 | -30°07'31".4 | 1.619 | 17.156 | 0.343 | 0.296 | 2.396601 |
| 38 | 3532 | 18 ^h 01 ^m 10 ^s .10 | -29°46'17".9 | 1.795 | 17.420 | 0.357 | 0.207 | 6.338837 |
| 38 | 3758 | 18 ^h 02 ^m 00 ^s .41 | -29°44'30".0 | 1.634 | 17.102 | 0.234 | 0.076 | 4.501576 |
| 38 | 4718 | 18 ^h 01 ^m 24 ^s .01 | -29°33'20".9 | 1.868 | 16.910 | 0.330 | 0.106 | 4.589060 |
| 38 | 5059 | 18 ^h 01 ^m 57 ^s .05 | -29°30'27".5 | 2.193 | 16.816 | 0.108 | 0.105 | 3.617376 |
| 39 | 511 | 17 ^h 56 ^m 01 ^s .79 | -30°08'43".3 | 2.124 | 17.210 | 0.323 | 0.143 | 2.220596 |
| 39 | 1893 | 17 ^h 55 ^m 08 ^s .38 | -29°56'48".4 | 1.872 | 17.722 | 0.396 | 0.146 | 2.452596 |
| 39 | 2555 | 17 ^h 55 ^m 24 ^s .39 | -29°52'20".7 | 2.389 | 17.157 | 0.288 | 0.200 | 2.879248 |
| 39 | 2745 | 17 ^h 55 ^m 16 ^s .18 | -29°50'20".9 | 2.168 | 16.717 | 0.313 | 0.088 | 8.139266 |
| 39 | 3008 | 17 ^h 55 ^m 31 ^s .48 | -29°48'50".6 | 2.772 | 18.302 | 0.268 | 0.154 | 3.591320 |
| 39 | 4483 | 17 ^h 55 ^m 25 ^s .33 | -29°38'32".6 | 2.412 | 18.056 | 0.245 | 0.165 | 4.946640 |
| 39 | 5279 | 17 ^h 55 ^m 15 ^s .81 | -29°32'08".1 | 1.833 | 16.698 | 0.306 | 0.118 | 5.776876 |
| 39 | 5315 | 17 ^h 55 ^m 37 ^s .41 | -29°31'44".2 | 1.905 | 18.374 | 0.292 | 0.180 | 2.048580 |
| 39 | 6095 | 17 ^h 55 ^m 19 ^s .90 | -29°26'12".8 | 2.106 | 17.206 | 0.388 | 0.236 | 2.885993 |
| 39 | 6554 | 17 ^h 56 ^m 05 ^s .16 | -29°23'08".8 | 2.351 | 18.098 | 0.312 | 0.228 | 2.144490 |
| 40 | 1732 | 17 ^h 51 ^m 09 ^s .87 | -33°19'16".9 | 2.229 | 16.557 | 0.351 | 0.250 | 2.934772 |
| 40 | 1808 | 17 ^h 50 ^m 54 ^s .17 | -33°18'35".6 | 2.199 | 17.029 | 0.370 | 0.259 | 2.465588 |
| 41 | 207 | 17 ^h 52 ^m 06 ^s .31 | -33°31'42".0 | 2.280 | 16.931 | 0.440 | 0.241 | 9.307920 |
| 41 | 279 | 17 ^h 52 ^m 37 ^s .85 | -33°30'41".5 | 1.833 | 18.366 | 0.196 | 0.139 | 2.583558 |
| 41 | 1414 | 17 ^h 52 ^m 15 ^s .20 | -33°14'55".5 | 2.076 | 17.974 | 0.312 | 0.148 | 2.544096 |
| 41 | 1593 | 17 ^h 52 ^m 35 ^s .87 | -33°13'14".6 | 2.074 | 17.135 | 0.409 | 0.225 | 6.934563 |
| 42 | 872 | 18 ^h 09 ^m 09 ^s .69 | -27°09'24".1 | 2.014 | 17.096 | 0.242 | 0.120 | 2.083840 |
| 42 | 875 | 18 ^h 09 ^m 11 ^s .46 | -27°09'32".6 | 1.852 | 17.414 | 0.239 | 0.110 | 4.297795 |
| 42 | 1309 | 18 ^h 09 ^m 08 ^s .77 | -27°03'57".7 | 1.706 | 16.405 | 0.446 | 0.261 | 4.606988 |
| 42 | 4197 | 18 ^h 09 ^m 17 ^s .51 | -26°26'31".4 | 2.056 | 17.903 | 0.416 | 0.158 | 2.161317 |
| 42 | 4324 | 18 ^h 08 ^m 55 ^s .48 | -26°25'19".7 | 1.976 | 15.675 | 0.373 | 0.224 | 2.452289 |
| 43 | 305 | 17 ^h 34 ^m 47 ^s .64 | -27°32'53".8 | 2.926 | 18.133 | 0.267 | 0.174 | 6.457909 |
| 43 | 310 | 17 ^h 35 ^m 04 ^s .55 | -27°32'29".1 | 2.706 | 18.111 | 0.348 | 0.223 | 6.223798 |
| 43 | 834 | 17 ^h 34 ^m 45 ^s .85 | -27°22'45".7 | 2.998 | 18.724 | 0.349 | 0.309 | 2.242491 |
| 43 | 1023 | 17 ^h 35 ^m 38 ^s .97 | -27°19'56".0 | 2.769 | 18.727 | 0.410 | 0.216 | 2.140171 |
| 43 | 2852 | 17 ^h 35 ^m 40 ^s .60 | -26°53'12".4 | 2.654 | 17.204 | 0.306 | 0.263 | 4.098304 |
| 44 | 2264 | 17 ^h 49 ^m 11 ^s .53 | -30°10'08".3 | 3.519 | 18.243 | 0.152 | 0.117 | 3.218736 |
| 46 | 178 | 18 ^h 04 ^m 24 ^s .67 | -30°28'10".5 | 1.874 | 16.991 | 0.311 | 0.156 | 3.379805 |
| 46 | 1863 | 18 ^h 04 ^m 26 ^s .40 | -29°42'49".6 | 1.402 | 16.447 | 0.137 | 0.077 | 5.429178 |
| 46 | 1982 | 18 ^h 04 ^m 46 ^s .68 | -29°39'41".2 | 1.796 | 16.902 | 0.371 | 0.227 | 3.712870 |
| 46 | 2039 | 18 ^h 04 ^m 16 ^s .65 | -29°37'23".5 | 2.096 | 15.451 | 0.401 | 0.201 | 2.679111 |
| 48 | 911 | 17 ^h 28 ^m 30 ^s .26 | -39°21'47".3 | 1.924 | 16.172 | 0.376 | 0.264 | 3.618835 |

Table 2

Parameters for the gold (1st part) and silver (2nd part) of the identified RG eclipsing binary pairs

| Field | ID | e | E_2 | t_1 [d] | $\sin i$ | Field | ID | e | E_2 | t_1 [d] | $\sin i$ |
|-------|------|-------|------------|-----------|----------|-------|------|-------|------------|-----------|----------|
| 3 | 2325 | 0.146 | 2450000.18 | 0.53 | 0.934 | 3 | 1149 | 0.043 | 2450002.60 | 0.43 | 0.932 |
| 3 | 2823 | 0.016 | 2449999.60 | 0.41 | 0.996 | 3 | 1688 | 0.113 | 2450002.78 | 0.30 | 0.993 |
| 3 | 2929 | 0.007 | 2450002.04 | 0.41 | 0.982 | 3 | 2195 | 0.113 | 2449999.43 | 0.41 | 0.912 |
| 3 | 7715 | 0.085 | 2450000.38 | 0.64 | 0.978 | 3 | 3488 | 0.141 | 2450000.73 | 0.18 | 1.000 |
| 4 | 830 | 0.062 | 2450002.58 | 0.91 | 0.915 | 3 | 3489 | 0.161 | 2450000.85 | 0.27 | 0.999 |
| 4 | 831 | 0.071 | 2450000.26 | 0.30 | 0.999 | 3 | 3547 | 0.143 | 2450000.24 | 0.21 | 0.988 |
| 4 | 1290 | 0.105 | 2450003.48 | 0.45 | 0.995 | 3 | 3744 | 0.103 | 2450001.63 | 0.37 | 0.964 |
| 5 | 1889 | 0.133 | 2449998.25 | 0.81 | 0.985 | 3 | 6413 | 0.169 | 2450005.48 | 0.87 | 0.978 |
| 7 | 1089 | 0.049 | 2450001.36 | 0.31 | 1.000 | 3 | 8222 | 0.212 | 2450006.10 | 0.72 | 0.983 |
| 9 | 132 | 0.150 | 2450001.36 | 0.43 | 0.947 | 3 | 8395 | 0.088 | 2449999.98 | 0.71 | 0.990 |
| 9 | 1502 | 0.008 | 2450002.67 | 0.42 | 0.984 | 4 | 1047 | 0.061 | 2450001.89 | 0.21 | 0.975 |
| 13 | 1282 | 0.036 | 2450000.63 | 0.99 | 0.990 | 4 | 1120 | 0.326 | 2450004.47 | 1.02 | 0.941 |
| 14 | 3912 | 0.189 | 2450001.04 | 0.61 | 0.974 | 4 | 1224 | 0.340 | 2450000.85 | 0.61 | 0.987 |
| 24 | 1374 | 0.310 | 2450000.38 | 0.61 | 0.943 | 4 | 1289 | 0.006 | 2450000.10 | 0.30 | 0.991 |
| 24 | 2461 | 0.009 | 2449990.80 | 2.25 | 0.955 | 4 | 3707 | 0.010 | 2450002.88 | 0.23 | 0.983 |
| 30 | 1600 | 0.009 | 2450002.26 | 0.41 | 0.977 | 4 | 4049 | 0.056 | 2450000.30 | 0.15 | 0.995 |
| 30 | 6658 | 0.061 | 2450007.81 | 1.11 | 0.960 | 4 | 4449 | 0.283 | 2450002.19 | 0.39 | 0.925 |
| 31 | 631 | 0.270 | 2450002.81 | 0.46 | 0.981 | 4 | 4564 | 0.098 | 2450001.56 | 0.35 | 0.987 |
| 31 | 2641 | 0.022 | 2450002.04 | 0.49 | 0.992 | 4 | 5392 | 0.043 | 2450001.82 | 0.15 | 0.991 |
| 34 | 1369 | 0.030 | 2450000.31 | 0.79 | 0.988 | 4 | 6839 | 0.004 | 2450000.51 | 0.24 | 0.961 |
| 34 | 6500 | 0.091 | 2450002.73 | 0.39 | 0.996 | 4 | 6905 | 0.028 | 2450001.74 | 0.34 | 0.981 |
| 37 | 1846 | 0.048 | 2450000.90 | 0.32 | 0.941 | 4 | 7346 | 0.128 | 2450002.42 | 0.28 | 0.996 |
| 37 | 6396 | 0.077 | 2450002.06 | 0.72 | 0.967 | 4 | 8604 | 0.003 | 2449999.09 | 0.27 | 0.998 |
| 37 | 7093 | 0.057 | 2450002.88 | 0.55 | 0.985 | 5 | 5124 | 0.074 | 2450001.96 | 0.30 | 0.995 |
| 39 | 1159 | 0.160 | 2450002.16 | 0.52 | 0.986 | 6 | 358 | 0.585 | 2450001.97 | 0.27 | 0.993 |
| 39 | 1604 | 0.084 | 2450000.11 | 0.32 | 1.000 | 6 | 598 | 0.063 | 2450000.40 | 0.25 | 0.995 |
| 40 | 310 | 0.293 | 2450003.46 | 0.96 | 0.994 | 6 | 1214 | 0.191 | 2450003.06 | 0.77 | 0.951 |
| 40 | 621 | 0.149 | 2450006.12 | 0.96 | 0.953 | 6 | 1517 | 0.005 | 2450001.71 | 0.21 | 1.000 |
| 43 | 3095 | 0.015 | 2450001.83 | 0.54 | 0.957 | 7 | 299 | 0.037 | 2449999.88 | 0.11 | 1.000 |
| 45 | 1064 | 0.203 | 2450087.27 | 4.99 | 0.999 | 7 | 605 | 0.134 | 2450002.56 | 0.52 | 0.998 |
| 45 | 1155 | 0.008 | 2450004.72 | 0.55 | 0.997 | 7 | 1494 | 0.036 | 2450001.95 | 0.14 | 0.997 |
| 45 | 1522 | 0.054 | 2450002.05 | 0.28 | 0.993 | 8 | 430 | 0.149 | 2450001.26 | 0.46 | 0.969 |
| 45 | 2170 | 0.088 | 2450009.51 | 1.86 | 1.000 | 8 | 829 | 0.025 | 2450000.33 | 0.31 | 0.995 |
| 47 | 481 | 0.091 | 2450001.98 | 0.38 | 0.984 | 10 | 1924 | 0.095 | 2450000.11 | 0.28 | 1.000 |
| 1 | 1713 | 0.017 | 2450003.65 | 0.25 | 0.998 | 10 | 2053 | 0.076 | 2450002.24 | 0.37 | 0.990 |
| 1 | 2513 | 0.003 | 2450002.41 | 0.31 | 0.896 | 11 | 1231 | 0.017 | 2450004.38 | 0.41 | 0.995 |
| 1 | 2938 | 0.205 | 2449999.27 | 0.34 | 0.987 | 11 | 1934 | 0.077 | 2450004.78 | 1.06 | 0.986 |
| 1 | 3738 | 0.088 | 2450000.55 | 0.30 | 0.995 | 12 | 1664 | 0.007 | 2450001.58 | 0.16 | 0.999 |
| 1 | 3846 | 0.377 | 2450002.09 | 0.71 | 0.999 | 12 | 2249 | 0.029 | 2450002.26 | 0.23 | 1.000 |
| 1 | 3859 | 0.131 | 2450000.92 | 0.36 | 0.972 | 12 | 3118 | 0.054 | 2450002.24 | 0.19 | 1.000 |
| 2 | 892 | 0.284 | 2450001.93 | 0.59 | 0.965 | 13 | 515 | 0.494 | 2450000.50 | 0.15 | 0.991 |
| 2 | 1301 | 0.059 | 2450006.32 | 0.52 | 0.995 | 13 | 643 | 0.242 | 2450001.77 | 0.35 | 0.994 |
| 2 | 1800 | 0.161 | 2449999.68 | 0.22 | 0.995 | 13 | 748 | 0.005 | 2450000.69 | 0.18 | 0.996 |
| 2 | 2542 | 0.024 | 2450001.47 | 0.35 | 0.973 | 14 | 748 | 0.187 | 2450000.90 | 0.28 | 1.000 |
| 2 | 3673 | 0.450 | 2450012.14 | 1.33 | 1.000 | 14 | 842 | 0.097 | 2450006.78 | 0.42 | 0.981 |
| 2 | 3894 | 0.034 | 2450003.90 | 0.36 | 0.992 | 14 | 1246 | 0.533 | 2450009.26 | 0.86 | 1.000 |
| 2 | 4754 | 0.045 | 2449999.62 | 0.22 | 0.995 | 14 | 1360 | 0.159 | 2450002.40 | 0.47 | 1.000 |

Table 2

Continued

| Field | ID | e | E_2 | t_1 [d] | $\sin i$ | Field | ID | e | E_2 | t_1 [d] | $\sin i$ |
|-------|------|-------|------------|-----------|----------|-------|------|-------|------------|-----------|----------|
| 14 | 2296 | 0.075 | 2450002.07 | 0.19 | 0.995 | 21 | 4732 | 0.715 | 2450001.35 | 0.20 | 0.995 |
| 14 | 3223 | 0.031 | 2450001.18 | 0.26 | 0.991 | 21 | 6233 | 0.021 | 2450001.27 | 0.39 | 0.998 |
| 14 | 3755 | 0.165 | 2450001.69 | 0.21 | 0.971 | 21 | 6795 | 0.052 | 2450003.61 | 0.58 | 0.998 |
| 15 | 529 | 0.270 | 2449999.35 | 0.49 | 0.983 | 21 | 7051 | 0.070 | 2450000.94 | 0.28 | 0.999 |
| 15 | 631 | 0.027 | 2450000.15 | 0.26 | 1.000 | 21 | 7356 | 0.031 | 2450000.90 | 0.46 | 0.964 |
| 15 | 851 | 0.000 | 2450001.61 | 0.40 | 0.994 | 22 | 10 | 0.160 | 2450000.71 | 0.40 | 0.979 |
| 15 | 1341 | 0.014 | 2450001.42 | 0.17 | 0.995 | 22 | 114 | 0.238 | 2450000.75 | 0.60 | 0.988 |
| 15 | 2256 | 0.212 | 2450002.68 | 0.31 | 0.997 | 22 | 222 | 0.046 | 2450007.33 | 0.56 | 1.000 |
| 16 | 147 | 0.006 | 2450003.99 | 0.46 | 0.996 | 22 | 1335 | 0.020 | 2450001.18 | 0.27 | 0.958 |
| 16 | 443 | 0.099 | 2449999.72 | 0.27 | 0.993 | 22 | 2938 | 0.082 | 2450002.79 | 0.38 | 0.992 |
| 16 | 722 | 0.010 | 2450002.17 | 0.64 | 0.946 | 23 | 293 | 0.118 | 2450004.27 | 0.36 | 0.999 |
| 16 | 2304 | 0.081 | 2450002.34 | 0.40 | 0.981 | 23 | 1425 | 0.039 | 2449999.64 | 0.19 | 0.987 |
| 16 | 3066 | 0.180 | 2450002.01 | 0.39 | 0.998 | 23 | 1695 | 0.018 | 2449998.85 | 0.25 | 0.997 |
| 17 | 417 | 0.047 | 2450000.36 | 0.35 | 0.981 | 23 | 3566 | 0.130 | 2450000.91 | 0.29 | 0.984 |
| 17 | 1576 | 0.446 | 2450000.33 | 0.46 | 1.000 | 23 | 3832 | 0.042 | 2450036.01 | 5.55 | 0.983 |
| 17 | 1577 | 0.023 | 2450013.98 | 1.18 | 0.999 | 24 | 1797 | 0.422 | 2450007.07 | 0.93 | 0.985 |
| 17 | 2366 | 0.027 | 2450000.55 | 0.13 | 0.996 | 24 | 2166 | 0.234 | 2449999.78 | 0.65 | 0.978 |
| 17 | 4107 | 0.018 | 2450000.12 | 0.42 | 0.985 | 24 | 2463 | 0.001 | 2450002.76 | 0.24 | 0.991 |
| 18 | 667 | 0.751 | 2450006.28 | 0.52 | 1.000 | 25 | 425 | 0.031 | 2450003.26 | 0.32 | 1.000 |
| 18 | 1201 | 0.123 | 2449999.32 | 0.34 | 0.983 | 25 | 2256 | 0.309 | 2450003.19 | 0.55 | 0.972 |
| 18 | 2492 | 0.078 | 2450003.06 | 0.26 | 1.000 | 25 | 2800 | 0.069 | 2450001.64 | 0.36 | 1.000 |
| 18 | 3232 | 0.064 | 2450000.77 | 0.15 | 0.980 | 25 | 2836 | 0.084 | 2450001.06 | 0.24 | 0.962 |
| 18 | 3834 | 0.011 | 2450001.89 | 0.20 | 0.998 | 26 | 572 | 0.089 | 2450004.20 | 0.92 | 0.995 |
| 18 | 3942 | 0.077 | 2450004.24 | 0.35 | 0.989 | 26 | 946 | 0.040 | 2450000.45 | 0.19 | 0.990 |
| 18 | 4093 | 0.098 | 2449998.71 | 0.36 | 0.994 | 26 | 1376 | 0.001 | 2449999.56 | 0.22 | 0.997 |
| 18 | 4246 | 0.115 | 2450006.97 | 0.62 | 0.980 | 26 | 3703 | 0.319 | 2450001.69 | 0.10 | 0.999 |
| 18 | 4368 | 0.014 | 2450002.51 | 0.17 | 0.993 | 26 | 3875 | 0.003 | 2450001.59 | 0.09 | 1.000 |
| 19 | 3463 | 0.075 | 2450000.00 | 0.21 | 0.995 | 26 | 4375 | 0.001 | 2450002.85 | 0.19 | 0.993 |
| 19 | 4115 | 0.017 | 2450001.19 | 0.21 | 0.997 | 26 | 4395 | 0.002 | 2450001.02 | 0.20 | 0.999 |
| 20 | 508 | 0.236 | 2450006.39 | 0.70 | 0.978 | 27 | 323 | 0.117 | 2450000.94 | 0.08 | 0.998 |
| 20 | 625 | 0.038 | 2450002.39 | 0.18 | 0.981 | 27 | 646 | 0.012 | 2450000.57 | 0.38 | 0.968 |
| 20 | 726 | 0.106 | 2450000.04 | 0.36 | 0.933 | 27 | 1512 | 0.034 | 2450000.35 | 0.37 | 0.999 |
| 20 | 764 | 0.098 | 2450006.14 | 0.47 | 0.990 | 27 | 1587 | 0.578 | 2450001.80 | 0.20 | 0.992 |
| 20 | 1218 | 0.009 | 2450000.64 | 0.41 | 0.994 | 27 | 2801 | 0.079 | 2450004.85 | 0.35 | 0.992 |
| 20 | 3228 | 0.069 | 2450001.66 | 0.26 | 0.976 | 28 | 974 | 0.009 | 2450001.45 | 0.21 | 1.000 |
| 20 | 3507 | 0.006 | 2450001.63 | 0.28 | 0.973 | 28 | 1355 | 0.005 | 2450001.30 | 0.18 | 0.998 |
| 20 | 3703 | 0.027 | 2450003.29 | 0.45 | 1.000 | 29 | 491 | 0.396 | 2450002.76 | 0.38 | 0.931 |
| 20 | 3831 | 0.032 | 2449999.51 | 0.12 | 0.998 | 29 | 943 | 0.085 | 2450008.30 | 0.49 | 0.999 |
| 20 | 4260 | 0.065 | 2450002.41 | 0.28 | 1.000 | 29 | 1001 | 0.002 | 2450002.67 | 0.33 | 0.992 |
| 20 | 5428 | 0.056 | 2450003.17 | 0.19 | 0.993 | 29 | 1063 | 0.013 | 2450001.85 | 0.28 | 0.979 |
| 21 | 564 | 0.031 | 2450001.79 | 0.32 | 0.984 | 29 | 1149 | 0.071 | 2450001.20 | 0.60 | 0.980 |
| 21 | 1563 | 0.041 | 2450022.50 | 1.68 | 1.000 | 29 | 1755 | 0.186 | 2450005.32 | 1.46 | 0.929 |
| 21 | 1588 | 0.007 | 2450001.60 | 0.37 | 0.941 | 30 | 983 | 0.084 | 2450024.31 | 1.17 | 0.999 |
| 21 | 2360 | 0.304 | 2450000.75 | 0.57 | 0.909 | 30 | 1034 | 0.240 | 2450000.80 | 0.34 | 0.996 |
| 21 | 2601 | 0.066 | 2450000.03 | 0.23 | 0.987 | 30 | 1558 | 0.431 | 2450001.29 | 0.24 | 0.996 |
| 21 | 2750 | 0.009 | 2450002.00 | 0.23 | 0.996 | 30 | 2126 | 0.215 | 2450000.72 | 0.32 | 0.993 |
| 21 | 3596 | 0.034 | 2450003.44 | 0.49 | 1.000 | 30 | 2158 | 0.104 | 2449999.72 | 0.27 | 0.990 |

Table 2

Concluded

| Field | ID | e | E_2 | t_1 [d] | $\sin i$ | Field | ID | e | E_2 | t_1 [d] | $\sin i$ |
|-------|------|-------|------------|-----------|----------|-------|------|-------|------------|-----------|----------|
| 30 | 2508 | 0.080 | 2450002.46 | 0.54 | 0.993 | 37 | 2068 | 0.021 | 2449999.81 | 0.45 | 1.000 |
| 30 | 3167 | 0.034 | 2449999.87 | 0.17 | 0.997 | 37 | 2768 | 0.290 | 2450000.55 | 0.71 | 0.963 |
| 30 | 5566 | 0.015 | 2450002.92 | 0.26 | 1.000 | 37 | 3186 | 0.113 | 2450003.36 | 0.50 | 0.989 |
| 30 | 5978 | 0.140 | 2450009.17 | 0.56 | 1.000 | 37 | 3240 | 0.033 | 2449999.55 | 0.25 | 0.998 |
| 31 | 399 | 0.297 | 2450002.57 | 0.31 | 0.989 | 37 | 4541 | 0.255 | 2450003.12 | 0.40 | 0.957 |
| 31 | 2277 | 0.039 | 2450001.96 | 0.31 | 0.999 | 37 | 6333 | 0.006 | 2450000.15 | 0.27 | 0.995 |
| 31 | 2670 | 0.034 | 2450000.14 | 0.30 | 0.998 | 37 | 6549 | 0.033 | 2449999.94 | 0.23 | 0.994 |
| 31 | 2793 | 0.065 | 2450001.42 | 0.41 | 0.996 | 37 | 7240 | 0.043 | 2450000.94 | 0.19 | 0.999 |
| 31 | 3308 | 0.020 | 2450000.84 | 0.31 | 0.983 | 37 | 8237 | 0.176 | 2450003.66 | 0.53 | 0.990 |
| 31 | 4092 | 0.207 | 2450002.18 | 0.29 | 0.970 | 38 | 1003 | 0.092 | 2450002.94 | 0.25 | 0.986 |
| 31 | 4328 | 0.025 | 2450011.57 | 0.26 | 1.000 | 38 | 1675 | 0.065 | 2450000.27 | 0.26 | 0.992 |
| 31 | 4787 | 0.276 | 2450002.92 | 0.41 | 0.986 | 38 | 3532 | 0.395 | 2450002.55 | 0.72 | 0.985 |
| 32 | 926 | 0.002 | 2450008.44 | 0.47 | 1.000 | 38 | 3758 | 0.011 | 2450000.43 | 0.34 | 0.990 |
| 32 | 1504 | 0.062 | 2450003.01 | 0.57 | 0.998 | 38 | 4718 | 0.102 | 2450002.50 | 0.48 | 0.982 |
| 32 | 1928 | 0.063 | 2450000.06 | 0.60 | 0.945 | 38 | 5059 | 0.081 | 2450002.76 | 0.12 | 0.997 |
| 32 | 2053 | 0.009 | 2450005.37 | 0.41 | 0.999 | 39 | 511 | 0.084 | 2450000.16 | 0.23 | 0.984 |
| 32 | 3061 | 0.016 | 2450000.14 | 0.45 | 0.996 | 39 | 1893 | 0.124 | 2450000.19 | 0.31 | 1.000 |
| 32 | 3753 | 0.045 | 2449995.62 | 0.58 | 1.000 | 39 | 2555 | 0.069 | 2449999.00 | 0.26 | 0.990 |
| 32 | 4589 | 0.068 | 2449997.85 | 0.27 | 0.999 | 39 | 2745 | 0.041 | 2450001.87 | 0.81 | 0.990 |
| 33 | 547 | 0.198 | 2450002.33 | 0.42 | 0.984 | 39 | 3008 | 0.043 | 2450001.65 | 0.31 | 0.995 |
| 33 | 686 | 0.001 | 2450002.17 | 0.21 | 1.000 | 39 | 4483 | 0.202 | 2450001.10 | 0.39 | 0.997 |
| 33 | 1629 | 0.009 | 2450000.96 | 0.20 | 0.992 | 39 | 5279 | 0.000 | 2450001.24 | 0.56 | 0.971 |
| 33 | 2278 | 0.119 | 2450001.35 | 0.25 | 0.981 | 39 | 5315 | 0.408 | 2450001.96 | 0.19 | 1.000 |
| 33 | 3188 | 0.140 | 2450003.61 | 0.52 | 0.998 | 39 | 6095 | 0.241 | 2450002.80 | 0.35 | 0.972 |
| 34 | 420 | 0.087 | 2450002.23 | 0.20 | 0.993 | 39 | 6554 | 0.040 | 2450001.05 | 0.21 | 1.000 |
| 34 | 793 | 0.143 | 2449997.29 | 0.78 | 0.963 | 40 | 1732 | 0.003 | 2450001.15 | 0.33 | 0.987 |
| 34 | 1615 | 0.059 | 2450002.31 | 0.30 | 0.988 | 40 | 1808 | 0.096 | 2450000.97 | 0.29 | 0.951 |
| 34 | 1706 | 0.045 | 2450000.92 | 0.38 | 0.990 | 41 | 207 | 0.319 | 2450006.21 | 1.29 | 0.974 |
| 34 | 1951 | 0.004 | 2450000.78 | 0.22 | 0.997 | 41 | 279 | 0.164 | 2450001.33 | 0.16 | 1.000 |
| 34 | 2456 | 0.092 | 2450003.99 | 0.67 | 0.995 | 41 | 1414 | 0.099 | 2450003.28 | 0.25 | 0.986 |
| 34 | 2580 | 0.030 | 2450002.19 | 0.26 | 1.000 | 41 | 1593 | 0.366 | 2450005.00 | 0.89 | 0.970 |
| 34 | 2823 | 0.127 | 2450001.38 | 0.18 | 0.999 | 42 | 872 | 0.043 | 2450002.10 | 0.16 | 0.997 |
| 34 | 2973 | 0.058 | 2450000.71 | 0.37 | 0.958 | 42 | 875 | 0.035 | 2450000.46 | 0.33 | 0.993 |
| 34 | 5744 | 0.018 | 2450002.74 | 0.27 | 1.000 | 42 | 1309 | 0.292 | 2449999.94 | 0.63 | 0.908 |
| 35 | 2440 | 0.214 | 2450001.24 | 0.20 | 0.999 | 42 | 4197 | 0.031 | 2449999.61 | 0.28 | 0.964 |
| 35 | 2508 | 0.066 | 2450015.41 | 1.44 | 0.999 | 42 | 4324 | 0.019 | 2450000.87 | 0.29 | 0.974 |
| 35 | 2897 | 0.010 | 2450000.72 | 0.26 | 0.996 | 43 | 305 | 0.073 | 2450005.41 | 0.55 | 0.994 |
| 35 | 4121 | 0.045 | 2450001.93 | 0.35 | 0.985 | 43 | 310 | 0.207 | 2450004.46 | 0.69 | 1.000 |
| 35 | 4556 | 0.005 | 2449998.35 | 0.26 | 0.995 | 43 | 834 | 0.087 | 2450001.81 | 0.25 | 0.992 |
| 35 | 4721 | 0.300 | 2450000.12 | 0.28 | 0.982 | 43 | 1023 | 0.189 | 2450000.19 | 0.28 | 0.977 |
| 36 | 1929 | 0.108 | 2450001.57 | 1.06 | 0.975 | 43 | 2852 | 0.010 | 2450002.65 | 0.40 | 0.998 |
| 36 | 3762 | 0.822 | 2450000.63 | 0.11 | 1.000 | 44 | 2264 | 0.014 | 2450001.75 | 0.16 | 0.999 |
| 36 | 4333 | 0.015 | 2450001.79 | 0.49 | 1.000 | 46 | 178 | 0.044 | 2449999.81 | 0.33 | 1.000 |
| 36 | 4493 | 0.010 | 2450000.32 | 0.29 | 0.996 | 46 | 1863 | 0.139 | 2450005.16 | 0.24 | 1.000 |
| 36 | 4494 | 0.007 | 2450000.33 | 0.31 | 0.998 | 46 | 1982 | 0.148 | 2450000.30 | 0.44 | 0.993 |
| 36 | 7720 | 0.183 | 2450003.00 | 0.24 | 1.000 | 46 | 2039 | 0.041 | 2450000.66 | 0.33 | 0.937 |
| 37 | 956 | 0.127 | 2450001.54 | 0.35 | 0.999 | 48 | 911 | 0.093 | 2450002.22 | 0.43 | 0.988 |